RESEARCH ARTICLE

SLC5A3-Dependent Myo-inositol Auxotrophy in Acute Myeloid Leukemia

Yiliang Wei[1], Yu-Han Huang[1], Damianos S. Skopelitis[1], Shruti V. Iyer[1,2], Ana S.H. Costa[1], Zhaolin Yang[1], Melissa Kramer[1], Emmalee R. Adelman[3], Olaf Klingbeil[1], Osama E. Demerdash[1], Sofya A. Polyanskaya[1,4], Kenneth Chang[1], Sara Goodwin[1], Emily Hodges[5], W. Richard McCombie[1], Maria E. Figueroa[3], and Christopher R. Vakoc[1]

ABSTRACT

An enhanced requirement for nutrients is a hallmark property of cancer cells. Here, we optimized an *in vivo* genetic screening strategy in acute myeloid leukemia (AML), which led to the identification of the myo-inositol transporter SLC5A3 as a dependency in this disease. We demonstrate that SLC5A3 is essential to support a myo-inositol auxotrophy in AML. The commonality among SLC5A3-dependent AML lines is the transcriptional silencing of *ISYNA1*, which encodes the rate-limiting enzyme for myo-inositol biosynthesis, inositol-3-phosphate synthase 1. We use gain- and loss-of-function experiments to reveal a synthetic lethal genetic interaction between *ISYNA1* and *SLC5A3* in AML, which function redundantly to sustain intracellular myo-inositol. Transcriptional silencing and DNA hypermethylation of *ISYNA1* occur in a recurrent manner in human AML patient samples, in association with *IDH1/IDH2* and *CEBPA* mutations. Our findings reveal myo-inositol as a nutrient dependency in AML caused by the aberrant silencing of a biosynthetic enzyme.

SIGNIFICANCE: We show how epigenetic silencing can provoke a nutrient dependency in AML by exploiting a synthetic lethality relationship between biosynthesis and transport of myo-inositol. Blocking the function of this solute carrier may have therapeutic potential in an epigenetically defined subset of AML.

[1]Cold Spring Harbor Laboratory, Cold Spring Harbor, New York. [2]Stony Brook University, Stony Brook, New York. [3]Sylvester Comprehensive Cancer Center, Department of Human Genetics, University of Miami, Miller School of Medicine, Miami, Florida. [4]School of Biological Sciences, Cold Spring Harbor Laboratory, Cold Spring Harbor, New York. [5]Department of Biochemistry and Vanderbilt Genetics Institute, Vanderbilt University School of Medicine, Nashville, Tennessee.

Note: Supplementary data for this article are available at Cancer Discovery Online (http://cancerdiscovery.aacrjournals.org/).

Corresponding Author: Christopher R. Vakoc, Cold Spring Harbor Laboratory, 1 Bungtown Road, Cold Spring Harbor, NY 11724. Phone: 516-367-5030; E-mail: vakoc@cshl.edu

Cancer Discov 2022;12:450–67

doi: 10.1158/2159-8290.CD-20-1849

INTRODUCTION

A consistent property of cancer cells is metabolic dysfunction, which can occur to support the energetic and biosynthetic requirements of a rapidly growing tumor (1). One manifestation of this process is that tumor cells become more dependent on extracellular nutrient uptake for their growth and viability than do normal tissues, a process referred to as auxotrophy (2). In many tumors, auxotrophies are driven by an elevated anabolic demand for metabolite building blocks, as is the case for serine (3), glutamine (4), and cysteine (5). However, cancer cells can also develop nutrient dependencies through an acquired defect in *de novo* metabolite biosynthesis pathways. One of the clearest examples of this is the dependence of lymphoid cancers on extracellular asparagine, which occurs because the rate-limiting enzyme in asparagine biosynthesis becomes epigenetically silenced in this malignancy (6). This nutrient dependency can be exploited by infusion of recombinant asparaginase, which is an approved chemotherapeutic in acute lymphoblastic leukemia that depletes asparagine from the plasma (7). Arginine and cholesterol auxotrophies in cancer have also been attributed to diminished expression of key biosynthetic enzymes (8, 9). While these examples point to the therapeutic significance of auxotrophy in human cancer, few systematic surveys of nutrient dependencies have been performed in cancer to date.

Solute carriers (SLC) are an important class of transporter proteins that regulate nutrient utilization in normal and

neoplastic contexts. The human genome encodes over 400 SLC proteins organized into 65 subfamilies, which regulate intracellular levels of amino acids, sugars, ions, lipids, neurotransmitters, and drugs (10). SLCs contain transmembrane alpha helices that form a substrate binding channel, which often use ion gradients to cotransport substrates into cells (11). Genetic targeting of SLCs, owing to their specificity for transporting specific substrates, provides a powerful tool for manipulation of intracellular metabolite levels and for exploration of nutrient dependencies (12, 13). Numerous SLC genes are mutated in human genetic disorders, and an emerging body of evidence suggests a role for SLC proteins in the pathogenesis of human cancer (14–16). Moreover, the substrate binding cavity of SLC proteins can be blocked with small molecules, which has fueled an interest in this class of proteins as drug targets (16–18).

Myo-inositol is an abundant carbocyclic sugar alcohol in eukaryotic cells (19, 20). One of the most well-characterized functions of myo-inositol is as a head group component of lipid phosphatidylinositols (PI), which are important signaling molecules that function downstream of growth factor signaling. In this lipid context, the phosphorylation state of myo-inositol is highly regulated by kinases (e.g., PI3K) and phosphatases (e.g., PTEN) to control the AKT–mTOR signaling axis (21). In addition, phospholipase C can release inositol triphosphates from PIs, which function as a second messenger that promotes the intracellular release of calcium from the endoplasmic reticulum (22, 23). Myo-inositol is also an osmolyte, whose intracellular concentrations can be regulated to allow cells to survive in hypertonic environments (24, 25).

Intracellular myo-inositol can be derived from three different sources: (i) *de novo* biosynthesis from glucose (26, 27), (ii) regeneration from inositol phosphates via the action of phosphatases (28), or (iii) uptake from the extracellular environment by inositol transporters (29). For *de novo* biosynthesis, glucose is first phosphorylated by hexokinase, then converted to myo-inositol-1-phosphate by the enzyme inositol-3-phosphate synthase 1 (ISYNA1), and finally dephosphorylated by inositol monophosphatase to form free myo-inositol. Importantly, ISYNA1 catalyzes the rate-limiting step in myo-inositol biosynthesis (30). For extracellular uptake, there are three known myo-inositol SLC transporters in humans: SLC5A3 (31), SLC5A11 (32), and SLC2A13 (33). Both SLC5A3 and SLC5A11 are sodium ion–coupled inositol transporters, whereas SLC2A13 is a proton-coupled inositol transporter (29). Among these transporters, SLC5A3 is the most widely expressed across different tissues and has the highest affinity for myo-inositol (33–37).

In this study, we set out to identify genetic dependencies needed for the growth of acute myeloid leukemia (AML) cells *in vivo*. This approach identified the myo-inositol transporter SLC5A3 as an *in vivo*–relevant dependency unique to AML. We show that this dependency is caused by aberrant silencing of *ISYNA1*. While loss of *ISYNA1* has no detectable effect on the fitness of AML cells, it causes an enhanced dependency on SLC5A3 and on extracellular myo-inositol for cell viability. Taken together, our findings reveal myo-inositol auxotrophy as a metabolic vulnerability in AML.

RESULTS

A Domain-Focused CRISPR Screening Method for Identifying *In Vivo*–Relevant AML Dependencies

The genetic dependencies of a cancer cell can be markedly altered by *in vitro* versus *in vivo* growth conditions (38), particularly the requirement for cell-surface receptors and metabolic enzymes whose function is influenced by the extracellular microenvironment. This issue motivated us to develop a robust screening method for interrogating genetic dependencies of human AML cells grown *in vivo*. For this study, we employed our previously cloned domain-focused single-guide RNA (sgRNA) libraries targeting transcription factors (39), chromatin regulators (40, 41), and kinases (42). In addition, we cloned domain-focused sgRNA libraries targeting G-protein–coupled receptors, ion channels, SLCs, glycosyltransferases, proteases, and membrane proteins, which were all cloned into the LRG2.1T vector backbone that contains an optimized sgRNA2.1 scaffold (43). Our screens were performed by lentiviral transduction of each sgRNA library into the AML cell line MOLM-13, engineered to express caspase 9 (Cas9) and firefly luciferase. A key optimization step was to select for high engraftment efficiency of this MOLM-13 line through pretransplantation before running the pooled screen (Fig. 1A). After transduction with an sgRNA library, MOLM-13 cells were injected via tail vein into 10 to 20 immune-deficient mice. MOLM-13 cells were allowed to expand for 12 days *in vivo*, followed by the mice being sacrificed and genomic DNA being isolated from bone marrow and spleen tissue for deep sequencing of the PCR-amplified sgRNA cassette (Fig. 1A). While establishing this procedure, we found that pooling of bone marrow or spleen samples prior to PCR maximized sgRNA representation and the overall accuracy of the screens. Importantly, the sgRNA read count distribution (a reflection of screen quality) and the depletion pattern of control sgRNAs of *in vivo* samples were comparable with the same screen being performed *in vitro* (Supplementary Fig. S1; Supplementary Table S1). We have previously characterized AML dependencies *in vitro* using sgRNA libraries targeting kinases (42), transcription factors (39), and chromatin regulators (40, 41). The *in vivo* CRISPR screening showed highly consistent results with our previous findings (Fig. 1B–D). The *in vivo* screen results between pooled spleen and bone marrow samples were consistent as well (Supplementary Fig. S2). The overall accuracy of our screen was further supported by the *in vivo*–specific depletion of sgRNAs targeting *CD47* (44–46) and *CXCR4* (47), which are known AML dependencies that regulate interactions with the *in vivo* microenvironment (Fig. 1E). In contrast to previous *in vivo* RNA interference screening in leukemia that showed only approximately 10% of *in vivo* dependencies overlapping with *in vitro* targets (48), our screening showed largely consistent results between *in vivo* and *in vitro* conditions (Fig. 1F; Supplementary Fig. S3; Supplementary Table S1). From this screening effort targeting a total of 5,768 genes, we identified 239 targets as *in vivo*–relevant dependencies (Fig. 1F; Supplementary Table S1).

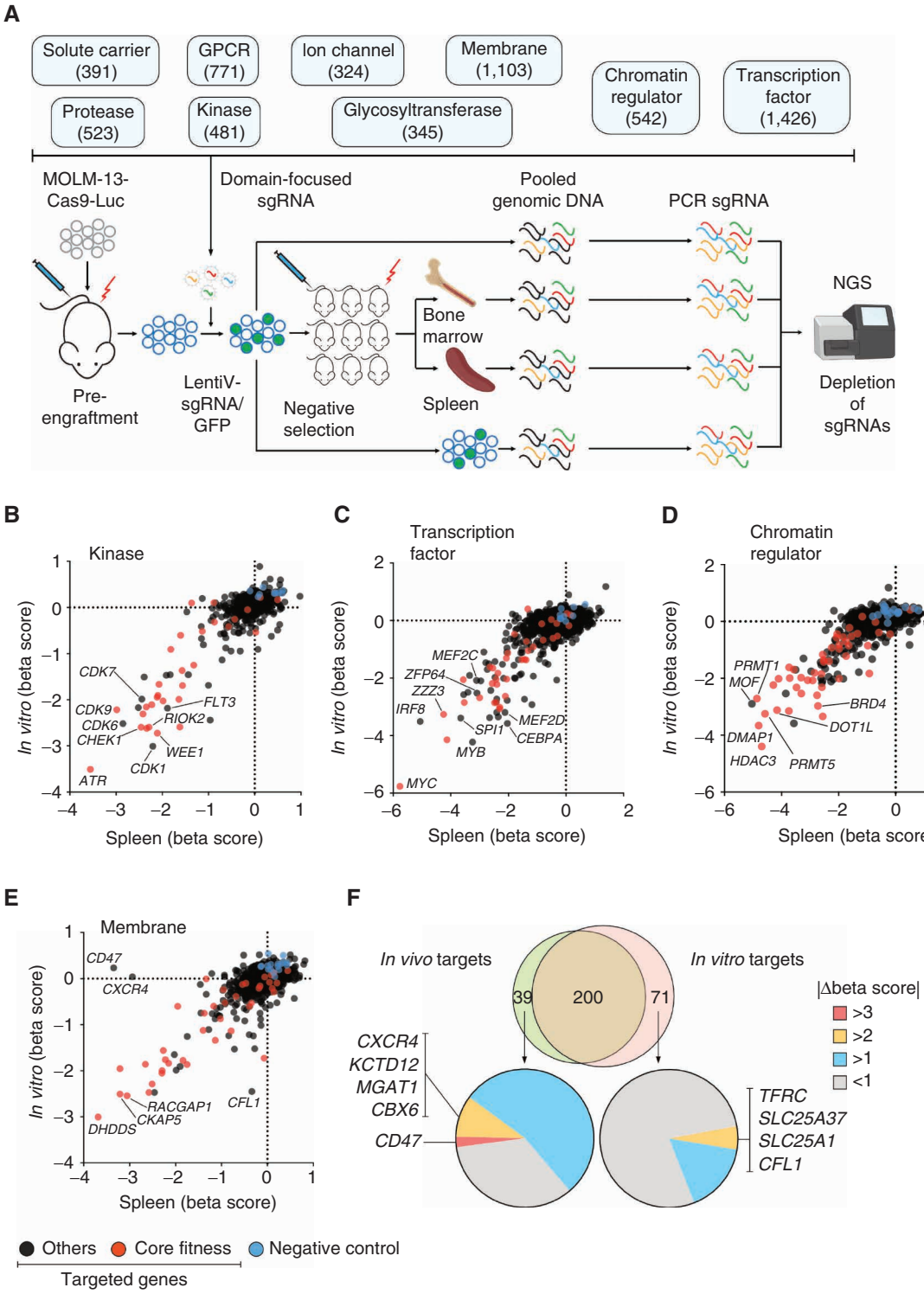

Figure 1. A domain-focused CRISPR screening method for identifying *in vivo*–relevant AML dependencies. **A,** Overview of *in vivo* genetic screening procedure using domain-focused sgRNA libraries. GPCR, G-protein–coupled receptor; NGS, next-generation sequencing. The numbers represent the number of genes in each sgRNA library. Images for mouse bone marrow, spleen, and NGS were created with a licensed version of BioRender. **B–E,** Examples of *in vivo* CRISPR screening results with sgRNA libraries targeting kinases (**B**), transcription factors (**C**), chromatin regulators (**D**), and membrane proteins (**E**). The gene beta score was calculated using MAGeCK (78, 79). The beta score describes how the gene knockout alters cell fitness: A positive beta score indicates positive selection, and a negative beta score indicates negative selection. The screening results using pooled spleen samples were compared with *in vitro* screening results. Core fitness genes (95) are in red; negative control sgRNAs are in blue. **F,** Venn diagram comparing genetic dependencies identified by *in vivo* screening with *in vitro* screening. The *in vivo*–relevant targets were determined using spleen data with $P < 0.05$, FDR < 0.25, and beta score < 0. For *in vivo*– and *in vitro*–specific targets, the absolute values of differential beta scores are shown as pie charts. Genes with a differential beta score of 2 or greater are listed.

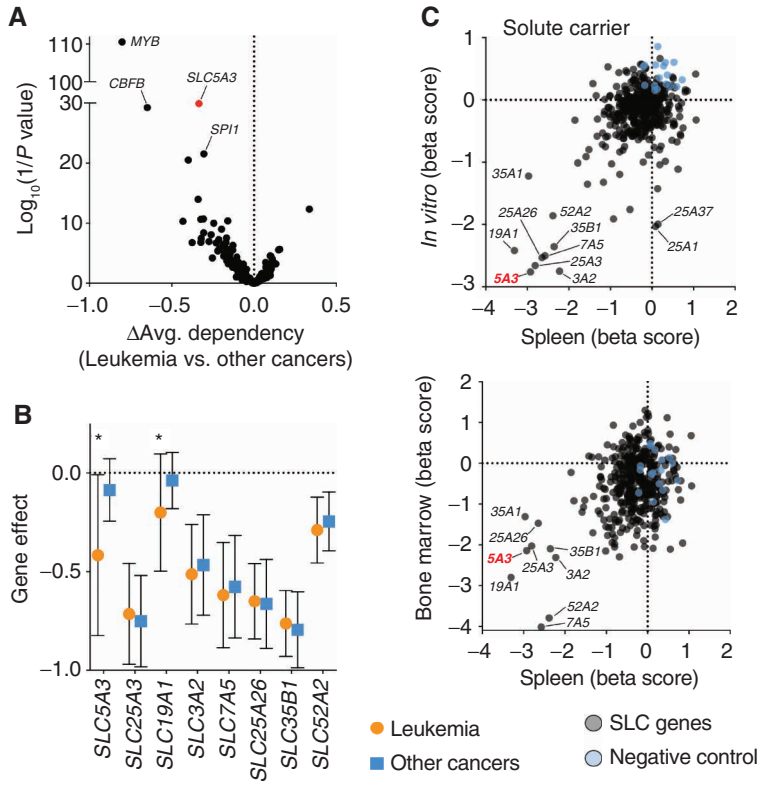

Figure 2. Dependency on SLC5A3 is *in vivo*–relevant and AML-specific. **A,** Analysis of Project Achilles genetic screening data, evaluating the leukemia-biased essentiality of 239 *in vivo*–relevant dependencies. The *in vivo* screening dependencies were determined by $P < 0.05$, FDR < 0.25, and beta score < 0. The average gene effect scores were calculated using Achilles Gene Effect 20Q3 data. The *P* values compared gene effect scores in leukemia versus other cancers using an unpaired Student *t* test. **B,** Comparison of dependencies of top SLC candidates between leukemia and other types of cancers. The dependency of SLC5A3 is the most leukemia-biased among the candidates. Data are obtained from DepMap database (20Q3). Plotted as average gene effect score with SD in leukemia cell lines versus nonleukemia cell lines. The *P* values were calculated using unpaired Student *t* test (*, $P < 0.05$). **C,** Summary of *in vivo* versus *in vitro* CRISPR screening results of the SLC sgRNA library.

SLC5A3 Dependency Is *In Vivo*–Relevant and AML-Specific

While our original intent was to identify *in vivo*–specific dependencies, the scarcity of such hits in our screen prompted us to explore instead whether any *in vivo*–validated dependencies were unique to AML relative to other cancers. For this purpose, we turned to Project Achilles/DepMap, which has performed genome-wide CRISPR screens for essential genes in more than 769 diverse cancer cell lines grown *in vitro* (49, 50). Through analysis of these data, we nominated myeloid lineage TFs (MYB, CBFB, and SPI1) and the myo-inositol transporter protein SLC5A3 as the top leukemia-biased dependencies among the pool of *in vivo*–validated targets (Fig. 2A). The AML specificity of SLC5A3 was distinct from other essential SLC genes, which tended to be needed across diverse cancer types (Fig. 2B). The *in vivo* screening in MOLM-13 cells and our own *in vitro* SLC screening in 10 diverse cancer cell lines corroborated SLC5A3 as a unique AML dependency under *in vitro* and *in vivo* conditions (Fig. 2C; Supplementary Fig. S4A–S4E). Unlike the aforementioned myeloid TFs, no prior study has investigated the role for SLC5A3 in AML, which motivated our subsequent evaluation of this target.

Validation of SLC5A3 Dependency in a Subset of AML Cell Lines

To validate SLC5A3 as a dependency in AML, we performed competition-based proliferation assays following lentiviral transduction with sgRNA-expressing vectors in Cas9-expressing AML cell lines. The genome editing efficiency of these sgRNAs targeting SLC5A3 was validated using genomic DNA qPCR with primers that hybridize to the Cas9 target sequence (Supplementary Fig. S5A). Using this approach, we validated that the cell fitness of several AML lines was impaired by SLC5A3 sgRNAs (e.g., MOLM-13, SEM, MV4-11, U937, EOL1), whereas other AML lines were SLC5A3 independent (e.g., HEL, KASUMI, SET2; Fig. 3A; Supplementary Fig. S5B and S5C). As a control, an sgRNA targeting the DNA replication protein PCNA suppressed the growth of all cancer cell lines tested (Fig. 3A; Supplementary Fig. S5B). cDNA rescue experiments also supported that these cell fitness alterations were due to a requirement for the *SLC5A3* gene product and ruled out off-target effects as contributing to this phenotype (Supplementary Fig. S6A–S6E). In MOLM-13 cells, loss of SLC5A3 led to cell-cycle arrest (Supplementary Fig. S7A and S7B). We also verified that knockout of *SLC5A3* suppressed the growth of MOLM-13 cells under *in vivo* conditions

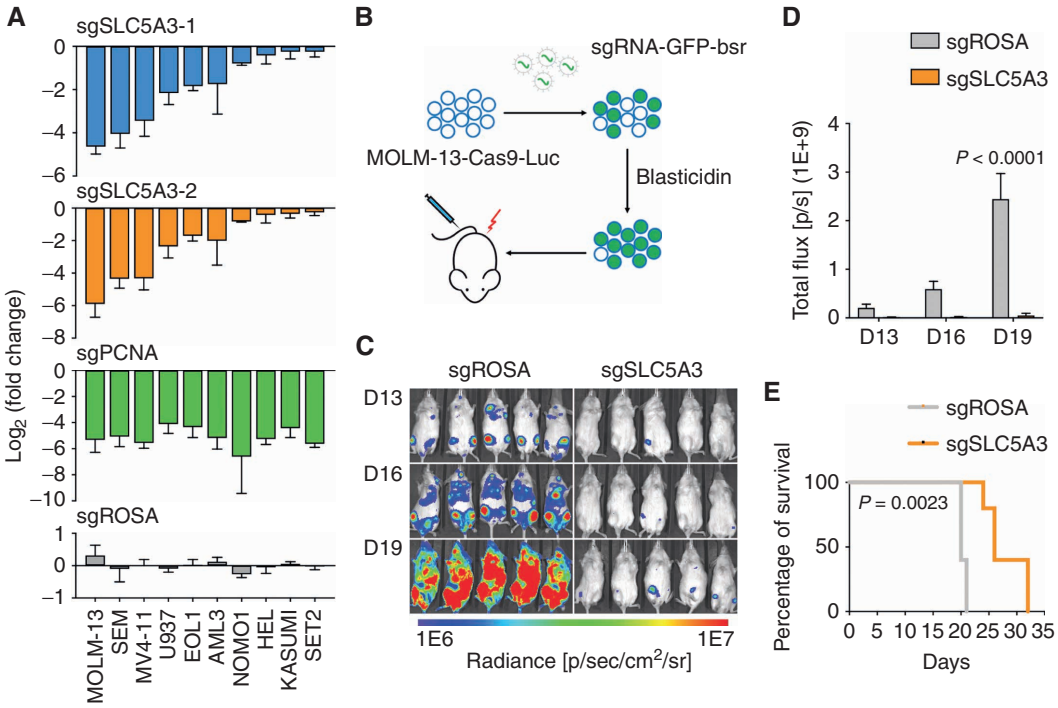

Figure 3. Validation of SLC5A3 dependency. **A,** Summary of *in vitro* validation experiments of individual sgRNAs (linked to GFP) in competition-based proliferation assays in AML cell lines. Plotted is the $\log_2$-transformed fold change of GFP-positive cell percentage at day 18 versus day 3 after infection of sgRNA lentivirus. Shown as mean with SD of two to seven biological replicates. **B,** Procedure of *in vivo* validation of SLC5A3 dependency in human AML. MOLM-13 cells expressing Cas9 and luciferase were transduced with sgROSA or sgSLC5A3-2 (linked to GFP/bsr) and then selected with blasticidin. The SLC5A3 knock-out cells (sgSLC5A3) and control cells (sgROSA) were then transplanted into NSG mice via tail vein injection. **C,** Bioluminescence imaging of NSG mice transplanted with MOLM-13 cells transduced with the indicated sgRNA. The images were taken on days 13, 16, and 19 posttransplantation. **D,** Quantification of bioluminescence from **C**. Values represent total flux as photons per second (mean ± SD). The *P* value was calculated using unpaired Student *t* test ($n = 5$). **E,** Survival curves of mice shown in **C**. The *P* value was calculated using log-rank (Mantel–Cox) test ($n = 5$).

(Fig. 3B–E; Supplementary Fig. S8A–S8F). Collectively, these findings demonstrate that SLC5A3 is essential in a subset of AML cell lines under *in vitro* and *in vivo* conditions.

SLC5A3-Dependent AML Lines Are Myo-inositol Auxotrophs

Since the primary substrate for SLC5A3 is myo-inositol (29), we performed LC/MS to measure intracellular myo-inositol levels in cancer cell lines following SLC5A3 inactivation. As expected, knockout of SLC5A3 in MOLM-13 or MV4-11 cells led to a significant reduction of intracellular myo-inositol, whereas the level of other metabolites (e.g., glutamine) was unaffected (Fig. 4A). This finding prompted us to evaluate the impact of removing myo-inositol from the media of AML cell lines. Remarkably, SLC5A3-dependent cell lines MOLM-13, MV4-11, and U937 slowed their growth following myo-inositol depletion, whereas the growth of SLC5A3-independent lines HEL, SET2, and K562 was unaffected by myo-inositol depletion (Fig. 4B and C). Taken together, these experiments suggest that SLC5A3 dependency is associated with a myo-inositol auxotrophy in AML.

It has been shown that developmental abnormalities in *Slc5a3*$^{-/-}$ mice can be rescued by providing supraphysiologic concentrations of myo-inositol in the diet, which can be transported into cells in a SLC5A3-independent manner via low-affinity transporters (51–53). This observation motivated us to perform analogous experiments in SLC5A3-dependent AML cell lines by supplementing normal growth media with additional myo-inositol. This revealed that an approximately fivefold increase in myo-inositol concentrations in regular growth media (RPMI) was sufficient to bypass the necessity of SLC5A3 in MOLM-13 and MV4-11 cell line contexts (Fig. 4D). These findings lend strong support that the essential function of SLC5A3 in AML is the transport of extracellular myo-inositol into the cell interior.

Transcriptional Silencing of ISYNA1 Leads to SLC5A3 Dependency through a Synthetic Lethal Genetic Interaction

We next investigated the mechanism underlying SLC5A3 dependency and myo-inositol auxotrophy in AML. Importantly, SLC5A3 dependency did not correlate with expression of SLC5A3 or silencing of the alternative myo-inositol transporters SLC5A11 and SLC2A13 (Supplementary Fig. S9A–S9C). Furthermore, triple-knockout experiments targeting SLC5A3, SLC5A11, and SLC2A13, failed to reveal evidence of redundancy (Supplementary Fig. S10A and S10B). These results led us to consider whether the myo-inositol auxotrophy in AML was due instead to an acquired defect in *de novo* myo-inositol biosynthesis (Fig. 5A). By analyzing the

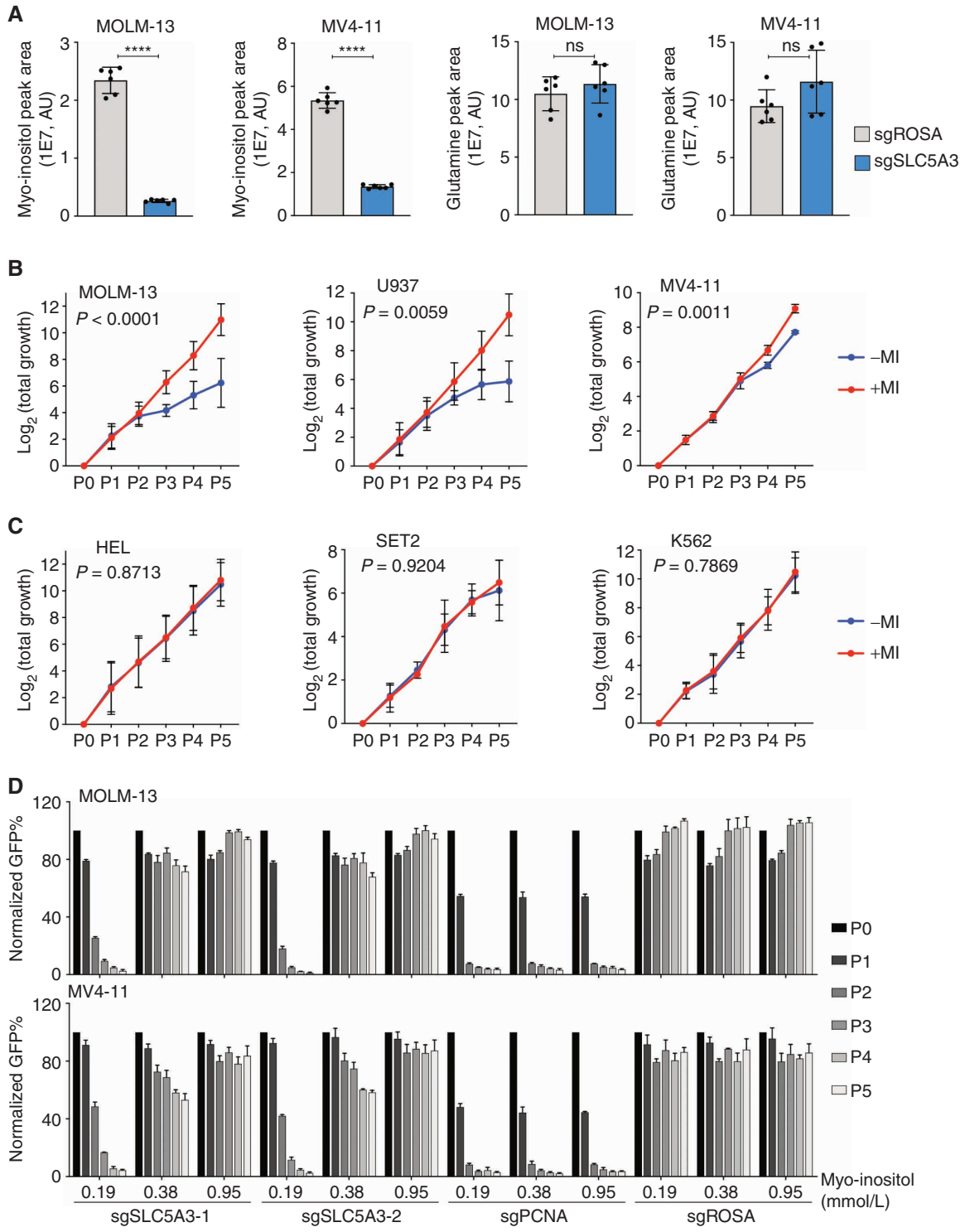

Figure 4. SLC5A3-dependent AML lines are myo-inositol auxotrophs. **A,** LC/MS analysis of cellular myo-inositol and glutamine levels in MOLM-13 and MV4-11 cells transduced with the indicated sgRNA. The *P* value was calculated using unpaired Student *t* test ($n = 6$; ****, $P < 0.0001$). ns, not significant. **B** and **C,** Depletion of myo-inositol in the cell culture medium affects the growth of SLC5A3-dependent lines MOLM-13, U937, and MV4-11 (**B**), but not SLC5A3-independent lines HEL, SET2, and K562 (**C**). A customized RPMI cell culture medium without myo-inositol, supplied with dialyzed FBS, was used (–MI). Additional myo-inositol supplement (1.11 mmol/L/0.2 g/L) was added into the medium for rescue (+MI). (Shown as mean with SD of two to four biological replicates; the *P* values were calculated using two-way ANOVA Sidak test to compare each line graph). **D,** Competition-based proliferation assays in MOLM-13 and MV4-11 cells transduced with the indicated sgRNA and treated with additional myo-inositol supplement. The base level of myo-inositol in RPMI medium is 0.035 g/L (0.19 mmol/L). To rescue the phenotype, additional myo-inositol was added to the cell culture to make myo-inositol concentration as 0.07 g/L (0.38 mmol/L) and 0.175 g/L (0.95 mmol/L). Myo-inositol from FBS (100% FBS contains ~0.9 mmol/L, determined by LC/MS, 10% FBS was added to cell culture medium) was not included (shown as mean with SD of three replicates with independent infections).

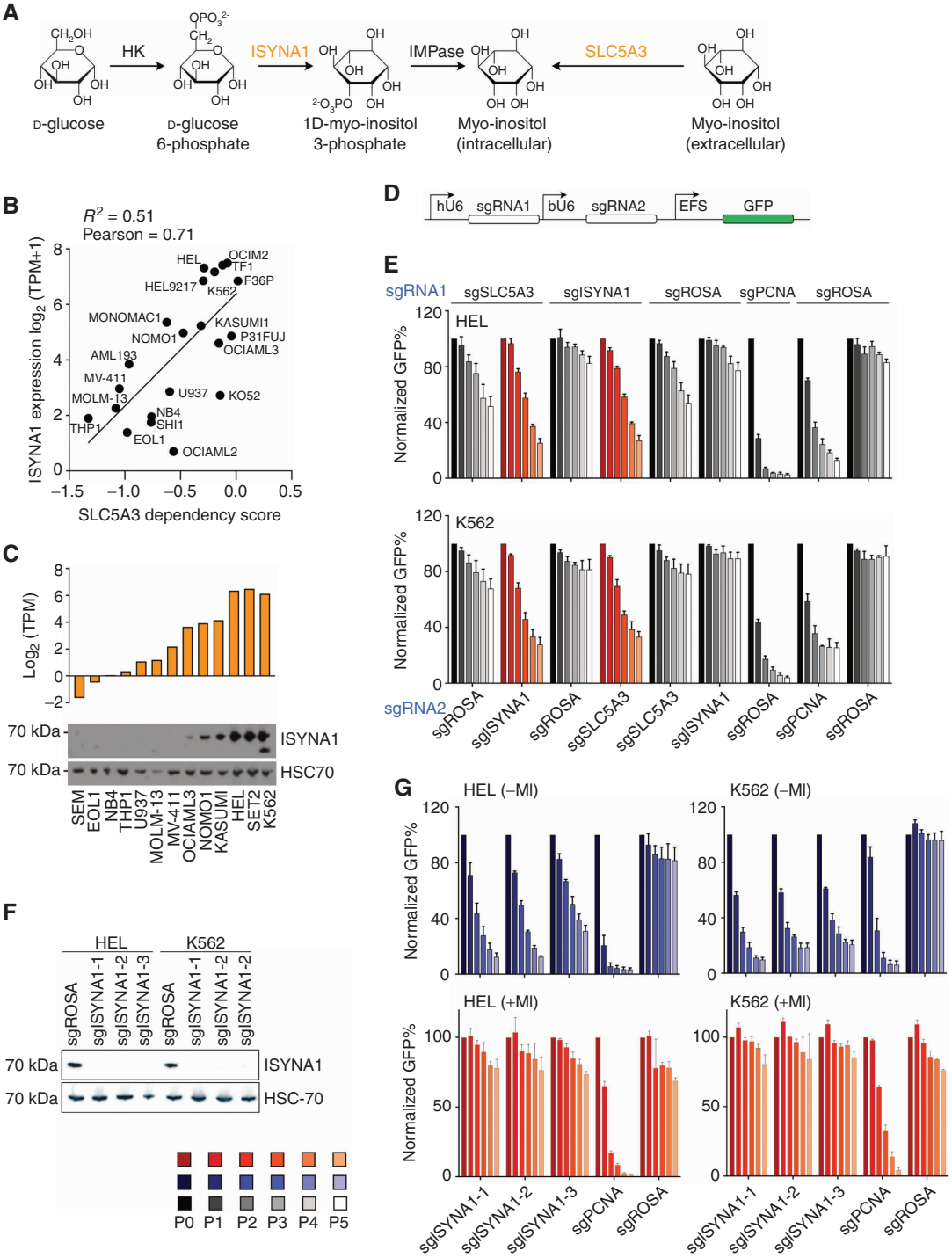

Figure 5. Transcriptional silencing of *ISYNA1* leads to SLC5A3 dependency through a synthetic lethal genetic interaction. **A,** Summary of two major sources of cellular myo-inositol: transported from extracellular environment by SLC5A3 and *de novo* biosynthesis from glucose. The rate-limiting *de novo* myo-inositol biosynthesis enzyme is inositol-3-phosphate synthase 1, encoded by the *ISYNA1* gene. **B,** SLC5A3 dependency in AML (and K562) cell lines correlates with ISYNA1 expression. Data from DepMap database (Achilles 20Q3). TPM, transcripts per kilobase million. **C,** Expression of ISYNA1 in AML (and K562) cell lines. The *ISYNA1* gene mRNA expression data were obtained from the Cancer Cell Line Encyclopedia (CCLE) database (96, 97). The ISYNA1 protein expression in AML lines and K562 (chronic myeloid leukemia) was detected by Western blot analysis, shown as one of two replicates. **D,** A double-knockout construct that cotargets two genes by two sgRNAs driven by the human U6 (hU6) or bovine U6 (bU6) promoter, respectively. The sgRNAs are linked to GFP. **E,** Competition-based proliferation assays in Cas9-expressing SLC5A3-independent cell lines following infection with the indicated cotargeting sgRNA constructs. Double knock-out both ISYNA1 and SLC5A3 leads to growth phenotype (red; shown as mean with SD of three replicates of independent infections.). **F,** Western blot shows depletion of the ISYNA1 protein in HEL and K562 cells following infection with the indicated sgRNA. **G,** Competition-based proliferation assays in Cas9-expressing HEL and K562 cells following infection with the indicated sgRNA. The experiment was performed in myo-inositol–deficient RPMI medium without myo-inositol supplement (–MI, blue), or with 0.05 g/L (0.28 mmol/L) myo-inositol supplement (+MI, red; shown as mean with SD of three replicates with independent infections).

mRNA levels of known myo-inositol biosynthesis genes, we noticed a significant inverse correlation between SLC5A3 dependency and expression of *ISYNA1*, which encodes the rate-limiting enzyme in myo-inositol biosynthesis (ref. 30; Fig. 5B). We confirmed the heterogeneous expression of ISYNA1 in AML cell lines using Western blotting, which mirrored the heterogeneity of mRNA levels (Fig. 5C; Supplementary Fig. S11A).

The findings above led us to hypothesize that a genetic redundancy may exist between *ISYNA1* and *SLC5A3*, which represent two independent strategies for maintaining intracellular myo-inositol levels. To evaluate this possibility, we targeted *ISYNA1* and *SLC5A3* (alone and in combination) in HEL and K562, which are leukemia lines that express both genes. Competition-based proliferation assays using biscistronic sgRNA vectors demonstrated that dual targeting of *ISYNA1* and *SLC5A3* led to a more severe proliferation defect than the loss of each gene individually (Fig. 5D and E; Supplementary Fig. S11B). LC/MS analysis demonstrated that a combined deficiency of ISYNA1 and SLC5A3 also led a more severe decrease in intracellular myo-inositol than observed following either single gene knockout (Supplementary Fig. S11C). Knockout of *ISYNA1* in HEL cells also led to a significant reduction of intracellular myo-inositol when cultured in myo-inositol–deficient media (Supplementary Fig. S11D). In addition, knockout of *ISYNA1* was sufficient to convert HEL and K562 cells into myo-inositol auxotrophs (Fig. 5F and G). Taken together, these experiments validate a genetic redundancy between ISYNA1 and SLC5A3 to sustain intracellular myo-inositol and cell viability.

To validate that ISYNA1 silencing is the underlying cause of myo-inositol auxotrophy and SLC5A3 dependency in AML, we lentivirally expressed a ISYNA1 cDNA in AML cell lines that lacked endogenous ISYNA1 expression (MOLM-13, MV4-11, EOL1, and U937; Fig. 6A). Remarkably, restoring ISYNA1 was sufficient to elevate myo-inositol levels and bypass the essentiality of SLC5A3 when cultured in normal growth media (Fig. 6B and C; Supplementary Fig. S12). This finding was further corroborated using a genome-wide screening approach, which revealed *SLC5A3* as the sole genetic dependency rescued by *ISYNA1* cDNA expression (Supplementary Fig. S13A–S13E). Furthermore, forced ISYNA1 expression eliminated the myo-inositol auxotrophy (Fig. 6D).

To validate that ISYNA1 is the key enzyme for *de novo* myo-inositol biosynthesis from glucose, we performed a stable isotope tracing experiment by treating the cells with ^{13}C-labeled glucose for 48 hours and measuring intracellular ^{13}C-labeled myo-inositol by LC/MS (Supplementary Fig. S14A). In MOLM-13 cells, the labeled glucose was converted into myo-inositol only when ISYNA1 was overexpressed (Supplementary Fig. S14B). On the contrary, a significant reduction of intracellular ^{13}C-labeled myo-inositol was observed in HEL cells following *ISYNA1* knockout (Supplementary Fig. S14C).

Aberrant *ISYNA1* Promoter Hypermethylation Occurs Recurrently in Human AML Patient Samples

We next evaluated whether epigenetic silencing of *ISYNA1* occurs in human AML patient samples. In the cell line AML models, we noticed that transcriptional silencing of *ISYNA1* was associated with DNA hypermethylation and the loss of histone acetylation in the vicinity of its CpG island/promoter (Supplementary Fig. S15A and S15B). Using Nanopore sequencing, we confirmed DNA hypermethylation at the *ISYNA1* gene in MOLM-13 and MV4-11 lines, as well as hypomethylation in the HEL line (Fig. 7A; Supplementary Fig. S15C). Notably, these regions remained unmethylated in normal human hematopoietic stem and progenitor cells (HSPC; ref. 54; Fig. 7A). Having established hypermethylation as a biomarker of *ISYNA1* silencing, we next evaluated whether this genomic region was hypermethylated in human AML patient samples analyzed by The Cancer Genome Atlas (TCGA), in which 170 genetically annotated samples were evaluated using Illumina Infinium 450k DNA methylation assay (55). In this study, we found that *ISYNA1* hypermethylation was present in approximately 20% of human AML samples (Z score > 0.5), whereas other flanking regions lacked heterogeneity in methylation (Fig. 7B; Supplementary Fig. S15D and S15E). Importantly, the presence of hypermethylation correlated with lower *ISYNA1* expression (Fig. 7C; Supplementary Fig. S15F). In addition, we found that *ISYNA1* hypermethylation was significantly enriched in patients with *IDH1*/*IDH2* or *CEBPA* mutations (Fig. 7B and D). The TCGA AML patient gene expression data further show that patients with *IDH2* mutations have significantly lower *ISYNA1* gene expression (Fig. 7E). We further evaluated *ISYNA1* methylation in an independent cohort of 119 AML patient samples analyzed using reduced representation bisulfite sequencing (56), which likewise identified hypermethylation in the *ISYNA1* genic region in a subset of AML cases, which was absent in normal bone marrow cells (Supplementary Fig. S16). Taken together, these findings validate that aberrant hypermethylation and silencing of *ISYNA1* occurs recurrently in AML.

DISCUSSION

Our study identifies myo-inositol auxotrophy as a previously unrecognized metabolic vulnerability in AML. We trace this auxotrophy to aberrant silencing of *ISYNA1*, which encodes the rate-limiting enzyme for myo-inositol biosynthesis. Our work suggests that normal cells maintain intracellular myo-inositol levels through the redundant mechanisms of *de novo* biosynthesis and SLC5A3-dependent transport from the extracellular microenvironment. Our work shows how *ISYNA1* silencing eliminates this redundancy, which in turn drives an elevated demand for SLC5A3-dependent myo-inositol transport in AML (Fig. 7F).

The evolution of redundant mechanisms for sustaining intracellular myo-inositol is likely to reflect the vital function of this metabolite, which is well supported by experiments in diverse eukaryotic species (57). Myo-inositol is incorporated as a head group into a variety of lipids that function to promote signal transduction in growth-promoting pathways (e.g., AKT–mTOR; ref. 21). Hence, blockade of SLC5A3 in ISYNA1-deficient AML is likely to extinguish AKT–mTOR signaling, which would be expected to cause an acute arrest in cell proliferation. Targeting SLC5A3 would also be expected to deplete the cell of inositol phosphates, which regulate

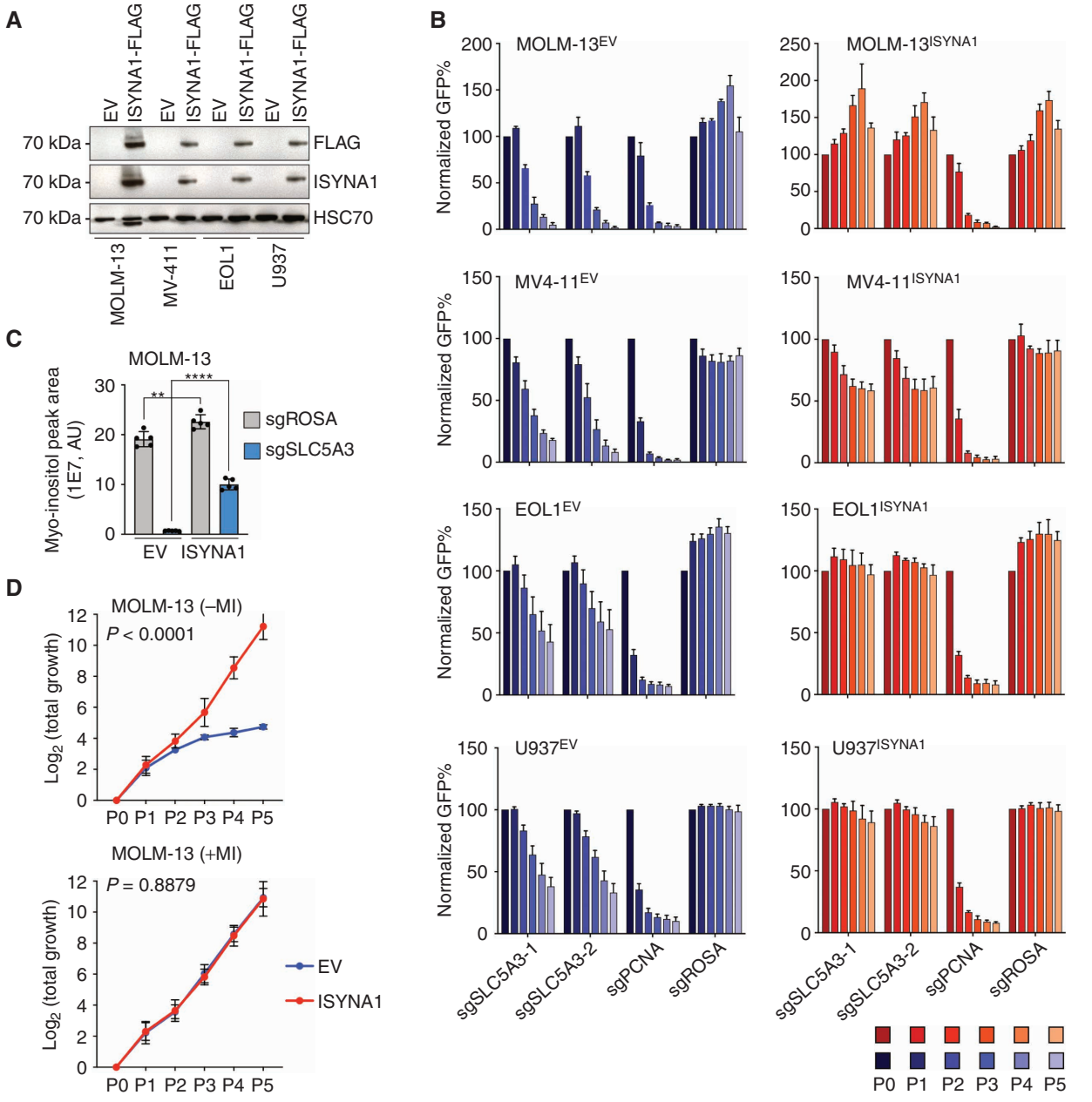

Figure 6. Reexpression of ISYNA1 eliminates SLC5A3 dependency and myo-inositol auxotrophy. **A,** Western blot shows overexpression of FLAG-tagged ISYNA1 in the indicated AML cell lines. **B,** Competition-based proliferation assays in SLC5A3-dependent AML lines expressing empty vector (EV, blue) or ISYNA1 (red), following infection with indicated sgRNA linked to GFP (shown as mean with SD of three replicates from independent infections). **C,** LC/MS analysis in MOLM-13 cells expressing empty vector or ISYNA1 following infection with indicated sgRNA. The *P* value was calculated using two-way ANOVA ($n = 5$; **, $P = 0.0011$; ****, $P < 0.0001$). **D,** Overexpression of ISYNA1 in MOLM-13 cells rescues the growth defect in myo-inositol deficient medium (–MI) but has no impact on the cell growth in medium with myo-inositol supplement (+MI; shown as mean with SD of two biological replicates; each includes three replicates with independent infection; the *P* value was calculated using two-way ANOVA Sidak test).

calcium release as well as the function of chromatin remodeling complexes (57, 58). These myriad functions of myo-inositol for cell viability are likely to contribute to the fitness defects of targeting SLC5A3 in AML.

Our study adds to a growing body of evidence highlighting how epigenetic silencing can alter metabolic pathways and lead to nutrient dependencies. Hypermethylation of the argininosuccinate synthetase (*ASS1*) gene promoter leads to an arginine dependency in several human cancers (8, 59, 60). Similarly, hypermethylation and silencing of asparagine synthetase (*ASNS*) has been linked to asparagine auxotrophy in lymphoid leukemia (6, 61, 62). Promoter hypermethylation of a rate-limiting cholesterol biosynthetic enzyme gene, squalene mono-oxygenase (*SQLE*), leads to cholesterol auxotrophy in anaplastic large-cell lymphoma (9). It remains unclear as to why the CpG islands of metabolic genes are prone to

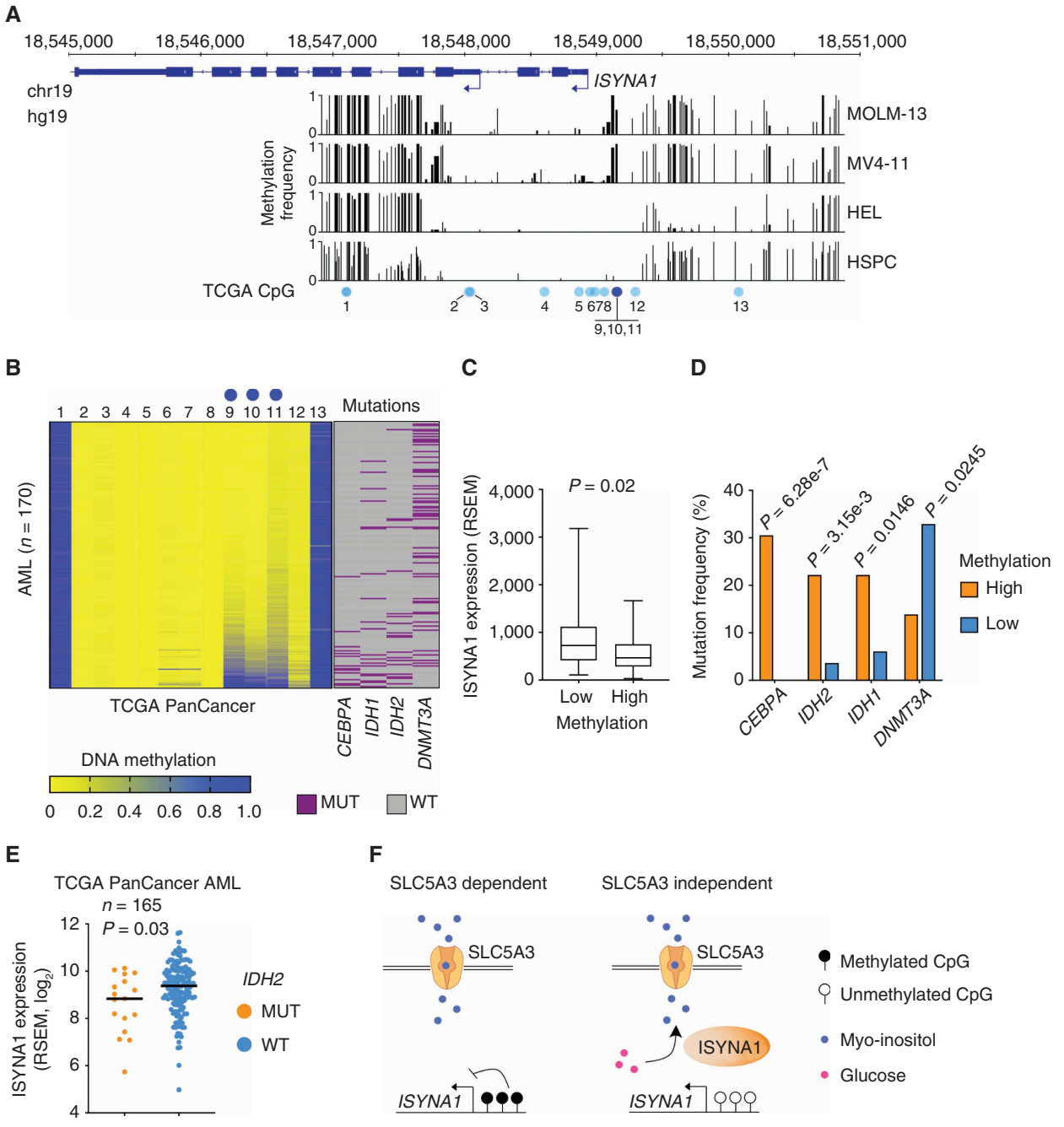

Figure 7. The *ISYNA1* gene is epigenetically silenced by aberrant DNA methylation in a subset of AML. **A** and **B,** CpG methylation status at the *ISYNA1* gene locus in AML cell lines (MOLM-13, MV4-11, HEL) and normal HSPCs (**A**), as well as patients with AML (**B**). The AML cell line methylation was measured by Nanopore sequencing. The HSPC methylation was measured by genome-wide bisulfite sequencing, obtained from a previous study (54). The AML patient data were obtained from the TCGA PanCancer AML database (55). The TCGA AML patient data used a DNA methylation array with reduced CpG representation, shown as "TCGA CpG" (blue dots). The CpGs at the ISYNA1 promoter (dark blue dots in TCGA CpG) show hypermethylated in SLC5A3-dependent/ISYNA1-low AML lines MOLM-13 and MV4-11, but hypomethylated in SLC5A3-independent/ISYNA1-high HEL line as well as normal HSPC cells. These regions were also shown aberrantly methylated in a subset of patients with AML (**B**). **C,** *ISYNA1* gene expression level is significantly lower in the high methylation group, compared with the low methylation group ($P = 0.02$). The high and low groups were determined by the Z scores of average DNA methylation levels of the three promoter CpGs (TCGA) described above (Supplementary Fig. S15E). **D,** *CEBPA*, *IDH1*, and *IDH2* mutations are enriched in the high *ISYNA1* methylation group, while *DNMT3A* mutation is enriched in the low methylation group. **E,** Patients with AML with *IDH2* mutations show lower *ISYNA1* gene expression ($P = 0.03$). Data in **D** and **E** were obtained from the TCGA PanCancer AML database via cBioPortal. **F,** A model depicting synthetic lethality between SLC5A3 and ISYNA1 in AML.

DNA hypermethylation, as it is unclear whether silencing of these genes confers a growth advantage in human cancer cells. Because epigenetic and metabolic regulation is tightly interconnected, it is possible that feedback regulation exists between the chromatin regulatory machinery and metabolite levels. For example, we observe that *ISYNA1*-silenced AML is correlated with the presence of *IDH1/IDH2* gain-of-function mutations, which produce 2-hydroxyglutarate, which in turn inhibits active DNA demethylation (63, 64). Thus, it is possible that the unique metabolic state of AML is the predisposing factor for *ISYNA1* silencing as a passenger epigenetic event in this disease—a possibility that warrants additional investigation.

The aberrant DNA methylation of *ISYNA1* is unlikely to be unique to AML, as several other cancer types (e.g., breast invasion carcinoma) we surveyed in the TCGA database also showed a similar pattern (Supplementary Fig. S17A–S17F). However, the correlation between SLC5A3 dependency and *ISYNA1* expression is weak in non-AML cell lines. This suggests that other factors might influence myo-inositol levels in non-AML contexts. Nevertheless, these findings raise the possibility that SLC5A3 dependency and myo-inositol auxotrophy might be present more broadly across human cancers.

Several mechanisms have been described by which the *ISYNA1* gene is regulated in mammalian cells to control myo-inositol biosynthesis, which may predispose to gene silencing in AML. For example, the inositol hexakisphosphate kinase 1 (IP6K1) has been found in the nucleus where it acts directly to maintain transcription of *ISYNA1* and prevent DNA hypermethylation (65). In addition, prior studies have shown that Musashi2, a known oncogene, regulates *ISYNA1* expression in the context of cancer (66). The tumor suppressor p53 has also been shown to directly regulate the *ISYNA1* promoter (67). Our own genetic analysis of human samples suggests that mutations of the C/EBPα transcription factor are associated with *ISYNA1* hypermethylation, which may influence the methylation state of this gene. Collectively, these studies suggest that several cancer-relevant pathways converge in regulating *ISYNA1* expression, which might underlie the aberrant silencing of this gene in AML.

Our work raises the possibility that the acquired dependency on SLC5A3 and extracellular myo-inositol in AML might have therapeutic significance. In analogy to the use of asparaginase in lymphoblastic leukemias (68), one possibility for therapeutic intervention in ISYNA1-deficient AML would be to suppress plasma levels of myo-inositol using an infusion of catabolic enzymes. MIOX (myo-inositol oxygenase) is one such enzyme that oxidizes myo-inositol into D-glucuronic acid (69, 70). Another enzyme capable of catabolizing myo-inositol is inositol dehydrogenase from *Bacillus subsilis* (71, 72). As an alternative strategy, several SLCs have been targeted using small molecules (15). Thus, an attractive strategy would be to suppress SLC5A3 function. While *Slc5a3*-null mice die soon after birth due to respiratory failure from abnormal development of peripheral nerves, this phenotype can be rescued by prenatal myo-inositol supplementation. Adult *Slc5a3*-null mice show a decrease of tissue myo-inositol levels and reduced nerve conduction velocity, which can also be alleviated by myo-inositol supplementation (52). Taken together, our findings justify an investigation of myo-inositol–lowering agents or SLC5A3 blockade as therapeutic interventions for the elimination of ISYNA1-deficient AML cells.

METHODS

Cell Lines and Culture

All cell lines were authenticated using short tandem repeat profiling. MOLM-13, MV4-11, SEM, OCIAML3, EOL1, U937, NOMO1, HEL, SET2, KASUMI1 (human AML), K562 (human chronic myeloid leukemia, CML), AsPC-1, MIA PaCa-2 (human pancreatic cancer), and NCI-H82 (human small-cell lung cancer, SCLC) cells were cultured in RPMI supplemented with 10% FBS. MA9-ITD and MA9-RAS (engineered human AML) cells were cultured in Iscove's modified Dulbecco's medium supplemented with 20% FBS (73, 74). RH30, RD (human rhabdomyosarcoma), and HEK293T cells were cultured in DMEM supplemented with 10% FBS. NCI-H1048 (human SCLC) was cultured in DMEM:F12 supplemented with 0.005 mg/mL insulin, 0.01 mg/mL transferrin, 30 nmol/L sodium selenite, 10 nmol/L hydrocortisone, 10 nmol/L β-estradiol, 4.5 mmol/L L-glutamine, and 5% FBS. Penicillin–streptomycin was added to all cell culture. All cell lines were cultured at 37°C with 5% CO_2, and were periodically tested negative for *Mycoplasma* contamination. All experiments were performed within 1 month of thawing a cryopreserved vial of cells.

To make myo-inositol–deficient cell culture, customized RPMI medium without myo-inositol (Bio-Techne) was supplemented with dialyzed FBS (#26400044, Thermo Fisher Scientific) and penicillin–streptomycin. The dialyzed FBS shows 100 times less myo-inositol level compared with regular FBS, as validated by LC/MS. To measure cell growth in myo-inositol–deficient cell medium as shown in Fig. 4, cells were washed twice with PBS to remove residue cell medium, and then resuspended in myo-inositol–deficient medium with 1 million cells per mL. Cells (1 mL) were transferred into one well in 12-well plates, with three replicates for each condition. Cell number and viability were measured using automated cell counter (Invitrogen Countess) every 2 days. For each passage, 0.4×10^6 (for MOLM-13 cells) or 0.2×10^6 (for other lines) cells were passed on to the next passage. For MOLM-13, MV4-11, and U937 lines that are sensitive to myo-inositol depletion, the cell numbers dropped drastically after a second or third passage in myo-inositol–deficient medium. For these samples, 1/5 volume of the cells were passed to the next passage. We performed at least two biological replicates (each included three technical replicates) for each cell line tested. For (+MI) cell medium, 0.2 g/L (1.11 mmol/L) myo-inositol (#I5125, Sigma) was added into the myo-inositol–deficient medium.

Animals

NOD.Cg-*Prkdc*^{scid} *Il2rg*^{tm1Wjl} Tg(CMV-IL3,CSF2,KITLG)1Eav/MloySzJ (known as NSGS) mice expressing human IL3, GM-CSF, and SCF were used for *in vivo* CRISPR screening. NOD.Cg-*Prkdc*^{scid} *Il2rg*^{tm1Wjl}/SzJ (known as NSG) mice were used for validating individual gene knockout *in vivo*. All animals were purchased from The Jackson Laboratory. Animal procedures and studies were reviewed and approved by the Institutional Animal Care and Use Committee at Cold Spring Harbor Laboratory (New York, NY).

Plasmid Construction

The lentiviral Cas9 vector (LentiV_Cas9_puro/Addgene #108100), the lentiviral sgRNA vectors (LRG2.1-GFP/Addgene #108098, LRG2.1-mCherry/Addgene #108099), the lentiviral luciferase vector (LentiV_Neo_Luc/Addgene #105621), and the lentiviral cDNA expression vector (LentiV_Neo/Addgene #108101) have been described in previous studies (42, 75). DNA oligos of the sgRNAs were cloned into LRG2.1-GFP/mCherry vectors using a *Bsm*BI restriction site. The cDNAs of *ISYNA1* (#OHu18552, GenScript) and *SLC5A3* (#53836,

Addgene) were cloned into LentiV_Neo vector using the In-Fusion cloning system (Takara Bio), and FLAG tag was inserted to the C-terminus of the cDNAs. The same system was used to mutate the protospacer adjacent motif (PAM) sequences in the *SLC5A3* gene. Dual targeting vectors were generated by inserting the sgRNA1-scaffold-bU6-sgRNA2 sequence (synthesized as gene blocks by IDT) into the *Bsm*BI site of the LRG2.1-GFP-P2A-BlastR vector using Gibson Assembly (NEB). The scaffold sequence for sgRNA1 was generated by replacing the stem–stem loop region of the LRG2.1 scaffold (76) with a previously described CRISPRi sgRNA scaffold (77).

Construction of a Domain-Focused sgRNA Library

The kinase sgRNA library and transcription factor sgRNA library have been described in previous studies (39, 42). The other sgRNA libraries were generated in a similar fashion. The gene lists were obtained from HUGO Gene Nomenclature Committee database (HGNC; https://www.genenames.org/). The domain-focused sgRNA libraries were designed by using the CSHL CRISPR sgRNA design tool (https://crispr.cshl.edu/), and at least six sgRNAs were selected for each gene or domain. Nontargeting sgRNAs as negative control and sgRNAs targeting essential genes as positive control were added into the pooled sgRNA library. The pooled library was synthesized on an array platform (Twist Bioscience) and then cloned into the *Bsm*BI restriction site of LRG2.1-GFP vector using Gibson Assembly (NEB).

Lentivirus Transduction

Lentivirus was produced in HEK293T cells as described in the previous study (42). Briefly, 10 μg of plasmid DNA was mixed with helper plasmids (5 μg VSVG and 7.5 μg psPAX2) and 1 mg/mL polyethylenimine (PEI 25000). The mix was then used to transfect HEK293T cells in a 10-cm dish. The mix was replaced by fresh cell media 6 hours after transfection, and lentivirus-containing supernatant was collected 24, 48, and 72 hours posttransfection. To infect cells with lentivirus, the target cells were mixed with the virus and 8 μg/mL polybrene in 12-well plates, and then centrifuged at 1,700 rpm for 45 to 60 minutes. Cell media was changed 24 hours postinfection. For cells infected with LentiV_Neo or LentiV_Blast vector, G418 or blasticidin was added to the cell culture at day 3 postinfection, respectively.

Pooled In Vivo CRISPR Screening

The Cas9- and Luciferase (Luc)-expressing MOLM-13 cell line (MOLM-13-Cas9-Luc) was established by infecting MOLM-13 cells with LentiV_Cas9_puro and LentiV_Neo_Luc, and then selected with puromycin and G418. To improve *in vivo* engraftment efficiency, 5 million MOLM-13-Cas9-Luc cells were transplanted into two sublethally irradiated (2.5 Gy), 8-week-old female NSG mice through tail vein injection. The cells were collected from the bone marrow of the injected mice 10 days postinjection by flushing the tibia with PBS. The collected cells were then cultured in RPMI supplemented with 10% FBS, puromycin, and G418 to remove murine cells.

To determine virus titer for the sgRNA library, MOLM-13-Cas9-Luc cells were infected with different volumes of the virus using the spin infection technique as described above. A flow cytometer (Guava easyCyte, Millipore) was used to determine the infection rate by measuring the percentage of GFP-positive cells. The amount of virus that gave approximately 30% infection rate was used for further infection experiments.

To ensure at least 1,000-fold coverage of each sgRNA in the library, the amount of cells to be infected was calculated using the equation: cell number = sgRNA number/infection rate × 1,000. For instance, given the sgRNA number in the SLC sgRNA library was approximately 3,000, and the infection rate was approximately 30%, at least 10 million cells were used for one CRISPR screening. Ten mice were planned to be injected, thus 1×10^6 cells were used for the initial infection.

To perform *in vivo* CRISPR screening, the pre-engraft MOLM-13-Cas9-Luc cells were infected with the library lentivirus. Three days postinfection, the infection rate was checked by flow cytometer to ensure approximately 30% GFP-positive cells. For the SLC sgRNA library, the infected wells were split into three groups. For group 1, 1×10^7 cells were spin-collected and kept frozen as P0. For group 2, 1×10^7 cells were kept growing in cell culture as *in vitro* CRISPR screening sample in parallel with *in vivo* CRISPR screening sample. During each passage, the percentage of GFP-positive cells was measured, and the cell number was calculated using the equation above to ensure at least 1,000-fold coverage of the sgRNA library. Group 3, 1×10^9 cells were collected, washed with PBS to remove any residual cell media, and then resuspended in 2 mL PBS (5×10^7 cells/mL). Two-hundred microliters of the cells were transplanted to one sublethally irradiated (2.5 Gy), 8-week-old female NSGS mouse via tail vein injection. A total of 9 mice were successfully injected. The engraftment and growth of the injected human AML cells were monitored by biofluorescence imaging (IVIS Spectrum System, Caliper Life Sciences). Images were taken 10 minutes after intraperitoneal injection of D-luciferin (50 mg/kg) every 3 days postinjection. On day 12 postinjection, the animals were euthanized. The spleen and bone marrow samples were collected. The spleen was broken down by gently crushing between the frost sides of two glass slides and then was filtered through a cell strainer. The bone marrow was flushed from the tibia by injecting with PBS. Meanwhile, the *in vitro* samples were also spin-collected. The genomic DNA from P0, *in vitro* sample, individual spleen and bone marrow were purified using QIAamp DNA Mini kit (Qiagen). The genomic DNA was then diluted into 100 ng/μL. An equal aliquot of genomic DNA from individual spleen and bone marrow were pooled to make pooled spleen and pooled bone marrow samples. The *in vivo* screening for other sgRNA libraries was performed in a similar fashion, with the amount of cells and the number of animals adjusted according to the sgRNA library size to ensure at least 1,000× coverage.

Barcoded sequencing libraries for P0, *in vitro*, 9 individual spleen, 9 individual bone marrow, pooled spleen, and pooled bone marrow samples were prepared using the same method as described in the previous study (42). The libraries were pooled and analyzed by paired-end sequencing using Miseq (Illumina) with MiSeq Reagent Kit v3 (Illumina).

The sequencing data were debarcoded and subsequently mapped to the reference sgRNA library using a customized tool as described in the previous study (76). The screening data were analyzed using MAGeCK-MLE (78, 79). A beta score was calculated for each gene and negative control by the MAGeCK-MLE model. It is a measurement of gene selections similar to log fold change in differential expression analysis (79). Negative beta score indicated negative selection, and positive beta score indicated positive selection. To calculate beta score for the nontargeting negative controls, every six negative controls were pooled as a single target for the MAGeCK-MLE calculation. The data were visualized using the Prism 8 program.

Pooled In Vitro CRISPR Screening

Ten cell lines representing five different types of cancers were used for *in vitro* CRISPR screening of the SLC sgRNA library, including MOLM-13, HEL, NOMO1 (AML), K562 (CML), AsPC-1, MIA PaCa-2 (pancreatic cancer), NCI-H82, NCI-H1048 (SCLC), RH30, and RD (rhabdomyosarcoma). The Cas9-expressing cell lines were established by infecting the cells with LentiV_Cas9_puro, and then selected with puromycin. The virus titer for each cell line was determined individually as described above. To ensure 1,000-fold coverage of the library, at least 1×10^7 cells were initially infected with the library with approximately 30% infection rate. Day 3 postinfection, 1×10^7 cells were collected and kept frozen as P0. Cells were passed every 3 days,

and cell number and GFP% were checked every passage. Cells collected at passages 5 and 8 were saved as P5 and P8 samples. Genomic DNA extraction, sequencing library preparation, and data analysis were performed as described above.

For the genome-wide CRISPR screens in Supplementary Fig. S13, Cas9-expressing MOLM-13 and MOLM-13^{ISYNA1} cells were transduced with Human CRISPR Knockout Pooled Library (Brunello, Addgene #73178) with low multiplicity of infection (~0.3). The original library vector contains puromycin selection marker, which was replaced with blasticidin-GFP selection marker. The transduced cells were selected with blasticidin and saved as P0. The cells were passaged for another 10 doublings and saved as P10. Two biological replicates were performed. Sequencing of the sgRNAs was performed on NextSeq platform. Data analysis was performed as described above.

Competition-Based Cell Proliferation Assay

Cas9-expressing cells were infected with sgRNA cloned into LRG2.1-GFP/mCherry or dual-targeting vector. The percentage of GFP- or mCherry-positive cells was first measured at day 3 postinfection (P0) by flow cytometer (Guava easyCyte, Millipore), and then measured every 2 to 3 days at each passage until passage 5 or 6. The relative fluorescent% for each passage was calculated using the equation: relative fluorescent% = [fluorescent%]/[P0 fluorescent%] × 100%. Decrease of the fluorescent% indicated the infected (gene knockout) cells were outcompeted by the uninfected (wild-type) cells.

Cell-Cycle Arrest Analysis

Cell-cycle analysis as shown in Supplementary Fig. S7 was performed according to the manufacturer's protocol (BD, FITC BrdU Flow Kit; #559619). Cells were pulsed with BrdU for 1 hour at 37°C and then were costained with 4′,6-diamidino-2-phenylindole (DAPI) for DNA content measurement. Cells were finally analyzed with a BD LSRFortessa flow cytometer (BD Biosciences) and FlowJo software (TreeStar). The experiments were performed in duplicates.

Western Blot Analysis

To detect ISYNA1 expression levels in human AML cell lines, 1×10^7 cells were collected, and cell pellets were resuspended in 500 μL 1X Laemmli sample buffer (Bio-Rad). The cell lysate was then boiled for 10 minutes, separated by SDS-PAGE, followed by transfer to nitrocellulose membrane and immunoblotting with 1:500 diluted mouse monoclonal anti-ISYNA1(C-9) antibody (#sc-271830, Santa Cruz Biotechnology) and then with 1:10,000 diluted polyclonal rabbit anti-mouse HRP antibody (#P0260, Agilent Dako). For control, mouse monoclonal anti-HSC70 (B-6) antibody (#sc-7298, Santa Cruz Biotechnology) was used with 1:10,000 dilution.

To detect the recombinant ISYNA1-FLAG, 1×10^7 cells were collected 2 weeks postinfection with cDNA vectors, followed by G418 selection. Protein sample preparation and immunoblotting were the same as described above. For FLAG-tagged proteins, 1:5,000 diluted mouse monoclonal anti-FLAG antibody (Sigma) was used, followed by a secondary antibody of rabbit anti-mouse HRP antibody (#P0260, Agilent Dako) with 1:10,000 dilution.

In Vivo *Validation Experiments*

For the *in vivo* validation as shown in Fig. 3, pre-engraft MOLM-13-Cas9-Luc cells were infected with LRG2.1-sgROSA-GFP-BlastR or LRG2.1-sgSLC5A3–2-GFP-BlastR. At day 2 postinfection, blasticidin was added to the cell culture to select for infected cells. After 3 days of selection, the cells were collected, washed with PBS to remove residual media, and resuspended to 1×10^6 cells/mL. One-hundred microliters of cells were transplanted to one sublethally irradiated (2.5 Gy), 8-week-old female NSG mouse via tail vein injection. Five mice were injected for each sgRNA. AML development was monitored by bioluminescence imaging (IVIS Spectrum System, Caliper Life Sciences). Images were taken 10 minutes after intraperitoneal injection of D-luciferin (50 mg/kg) on days 13, 16, and 19 postinjection.

For the *in vivo* validation as shown in Supplementary Fig. S8, pre-engraft MOLM-13-Cas9-Luc cells were infected with LRG2.1-sgROSA-GFP, LRG2.1-sgSLC5A3–1-GFP, LRG2.1-sgSLC5A3–2-GFP, LRG2.1-sgCD47–1-GFP, or LRG2.1-sgCD47–2-GFP. Excessive lentivirus was used to ensure more than 90% infection rate. The cells were then transplanted to NSG mice as described above.

Metabolomics Analysis by LC/MS

For the LC/MS analysis shown in Fig. 4, 0.5×10^6 cells were infected with LRG2.1-sgROSA-GFP-BlastR or LRG2.1-sgSLC5A3–2-GFP-BlastR in 12-well plates with six replicates. For the LC/MS analysis shown in Fig. 6, MOLM-13-Cas9 cells expressing empty vector (EV) or ISYNA1 were infected with LRG2.1-sgROSA-GFP-BlastR or LRG2.1-sgSLC5A3–2-GFP-BlastR in 12-well plates with five replicates. The infected cells were selected with blasticidin at day 2 postinfection for 3 days. For the LC/MS analysis shown in Supplementary Fig. S11–S11C, HEL-Cas9 and K562-Cas9 cells were infected with the indicated single- or dual-targeting sgRNA vectors with more than 90% infection rate, in 12-well plates with five replicates, for 5 days. The cells were then collected for sample preparation. For the LC/MS analysis shown in Supplementary Fig. S11–S11D, HEL-Cas9 cells were infected with LRG2.1-sgROSA-GFP-BlastR or LRG2.1-sgISYNA1-GFP-BlastR in 12-well plates with five replicates. The infected cells were selected with blasticidin at day 2 postinfection for 7 days. At least 95% of GFP-positive rate was achieved. The cells were then washed twice with PBS and cultured in myo-inositol–deficient medium for another 4 days before preparation for LC/MS.

To prepare cells for LC/MS, cells were quickly washed in PBS before adding 1 mL of ice-cold extraction solution (50% methanol, 30% acetonitrile, 20% H_2O) per 4×10^6 cells. The cells were then scrapped, and the suspension was snap frozen in liquid nitrogen. Samples were agitated using a Thermomixer (Eppendorf) at 1,400 rpm, 4°C for 15 minutes, followed by incubation at –80°C for 1 hour. Samples were then centrifuged at 15,000 rpm, 4°C for 10 minutes. The supernatants were further centrifuged for another 10 minutes. The supernatants were stored in autosampler vials at –80°C until analysis.

Intracellular extracts from five to six independent cell cultures were analyzed for each condition. Samples were randomized to avoid bias due to machine drift and processed blindly. LC/MS analysis was performed using a Vanquish Horizon UHPLC system coupled to a Q Exactive HF mass spectrometer (both Thermo Fisher Scientific). Sample extracts (5 μL) were injected onto a Sequant ZIC-pHILC column (150 mm × 2.1 mm, 5 μm) and a guard column (20 mm × 2.1 mm, 5 μm) from Merck Millipore kept at 45°C. The mobile phase was composed of 20 mmol/L ammonium carbonate with 0.1% ammonium hydroxide in water (solvent A) and acetonitrile (solvent B). The flow rate was set at 200 μL/minute with the previously described gradient (80). The mass spectrometer was operated in full MS and polarity switching mode. The acquired spectra were analyzed using XCalibur Qual Browser and XCalibur Quan Browser software (Thermo Fisher Scientific) by referencing to an internal library of compounds.

Stable Isotope Tracing by LC/MS

For tracing *de novo* myo-inositol synthesis from ^{13}C-labeled glucose as shown in Supplementary Fig. S14, ^{13}C-labeling medium was prepared by adding ^{13}C-labeled glucose (Sigma-Aldrich 389374; final concentration 2,000 mg/L) and dialyzed FBS (final concentration 10%) to glucose-free RPMI (Thermo Fisher Scientific 11879020). Cells were washed with PBS twice and seeded in 6-well plates with ^{13}C-labeling medium for 48 hours. Extracts from six independent cell cultures were analyzed for each condition. Briefly, after quick

removal of the culture medium, cells were washed in PBS before adding extraction solution (50% methanol, 30% acetonitrile, 20% H_2O). After centrifugation to remove the precipitated proteins and insoluble debris, the supernatants were collected and stored in autosampler vials at –80°C until analysis. Samples were randomized to avoid bias due to machine drift and processed blindly. LC/MS analysis was performed using a Vanquish Horizon UHPLC system coupled to a Q Exactive HF mass spectrometer (both Thermo Fisher Scientific). Sample extracts were analyzed as previously described (80). The acquired spectra were analyzed using XCalibur Qual Browser and XCalibur Quan Browser software (Thermo Fisher Scientific) by referencing to an internal library of compounds. Metabolite peak areas were corrected for natural ^{13}C abundance using the R package AccuCor (81). To calculate isotopolog distribution, corrected peak areas of each metabolite's isotopologs were normalized to the total metabolite pool (sum of all isotopologs of a given metabolite). Values of release of lactate were adjusted to cell density upon background subtraction.

Nanopore Sequencing

CRISPR RNA (crRNA) guides specific to the regions of interest (ROI) were designed as per recommended guidelines described in the Nanopore infosheet on Targeted, amplification-free DNA sequencing using CRISPR/Cas (Version: ECI_S1014_v1_revA_11Dec2018). The crRNA sequences are provided in Supplementary Table S2. Guides were reconstituted to 100 µmol/L using TE (pH 7.5) and pooled into an equimolar mix. For each distinct sample, four identical reactions were prepared in parallel using 5 µg gDNA each. Ribonucleoprotein complex (RNP) assembly, genomic DNA dephosphorylation, and Cas9 cleavage were performed as described in Gilpatrick and colleagues (82). Affinity-based Cas9-mediated enrichment (ACME) using Invitrogen His-Tag Dynabeads was performed to pull down Cas9-bound nontarget DNA, increasing the proportion of on-target reads in the sample (83). The resultant product was cleaned up using 1X Ampure XP beads (Beckman Coulter, #A63881), eluted in nuclease-free water, and pooled together. The ACME-enriched sample was quantified using Qubit fluorometer (Thermo Fisher Scientific) and carried forward to the adapter ligation step as described by Iyer and colleagues (83). Sequencing adapters from the Oxford Nanopore Ligation Sequencing Kit (ONT, SQK-LSK109) were ligated to the target fragments using T4 DNA ligase (NEBNext Quick Ligation Module E6056). The sample was cleaned up using 0.3X Ampure XP beads (Beckman Coulter, #A63881), washed with long-fragment buffer (LFB; ONT, SQK-LSK109), and eluted in 15 µL of elution buffer (EB; ONT, LSK109) for 30 minutes at room temperature. The resultant library was prepared for loading as described in the Cas9-mediated PCR-free enrichment protocol from ONT (Version: ENR_9084_v109_revH_04Dec2018) by adding 25 µL sequencing buffer (SQB; ONT, LSK109) and 13 µL loading beads (LB; ONT, LSK109) to 12 µL of the eluate. Each sample was run on a FLOMIN106 R9.4.1 flow cell using the GridION sequencer.

Real-time basecalling was performed with Guppy v3.2, and files were synced to our Isilon 400NL storage server for further processing on the shared CSHL high-performance computing cluster (HPCC). Nanopolish v0.13.2 (84) was used to call methylation as per the recommended workflow. Briefly, indexing was performed to match the ONT fastq read IDs with the raw signal level fast5 data. The ONT reads were then aligned to the human reference genome (UCSC hg38) using minimap2 v2.17 (85), and the resulting alignments were sorted with samtools v0.1.19 (86). Nanopolish call-methylation was then used to detect methylated bases within the targeted regions, specifically 5-methylcytosine in a CpG context. The initial output file contained the position of the CpG dinucleotide in the reference genome and the methylation call in each read. A positive value for log_lik_ratio was used to indicate support for methylation, using a cutoff value of 2.0. The helper script calculate_methylation.py was then used to calculate the frequency of methylation calls by genomic position.

qPCR Analysis of Indel Mutations

To analyze sgRNA editing of genomic DNA as shown in Supplementary Fig. S5A, cells were infected with LRG2.1-sgROSA-GFP-BlastR, LRG2.1-sgSLC5A3–1-GFP-BlastR, or LRG2.1-sgSLC5A3–2-GFP-BlastR. At day 2 postinfection, blasticidin was added to the cell culture to select for infected cells. After 3-day selection, the cells were collected, and genomic DNA was extracted using QIAamp DNA Mini kit (Qiagen). For qPCR, 20 to 25 ng of genomic DNA was used in each reaction with the indicated primer set. The C_t value of non–sgRNA-target primer was used to normalize the data. To analyze SLC5A3 (r-1 and r-2) expression as shown in Supplementary Fig. S6E, MOLM-13 cells were infected with the indicated cDNA constructs and were then selected with G418 for 2 weeks. Total RNA was extracted using TRIzol (Thermo Fisher Scientific), and cDNA was synthesized using qScript cDNA SuperMix (Quanta). All qPCR experiments were performed using Power SYBR Green PCR Master Mix (Thermo Fisher Scientific) on a QuantStudio Flex Real-time PCR machine (Thermo Fisher Scientific).

AML Patient Data

TCGA PanCancer AML patient data, including gene expression and mutation, were downloaded via cBioPortal (https://www.cbioportal.org/; refs. 87–89). The same patients' DNA methylation data were downloaded via NCI Genomic Data Commons (https://gdc.cancer.gov/; ref. 55). The AML (n = 119) and normal (n = 22) individual data from Glass and colleagues were downloaded from Gene Expression Omnibus (GEO; accession number GSE98350; ref. 56). After filtering and normalizing by coverage, a methylBase object containing the methylation information and locations of cytosines that were present in at least five samples per condition (meth.min = 5) was generated using MethylKit (version 1.9.3) and R statistical software (version 3.5.1). Percent methylation for each CG for each donor was calculated using the MethylKit "percMethylation" function. The Bedtools intersect function was used to determine overlap with CpG islands from hg19.

Chromatin Immunoprecipitation Sequencing Data Analysis

For chromatin immunoprecipitation sequencing (ChIP-seq) analysis shown in Supplementary Fig. S15A, raw reads were obtained from public GEO datasets, MOLM-13 (GSE63782/GSM1652920), K562 (GSE63782/GSM1652918; ref. 90), MV-411 (GSE79899/GSM2108039), THP-1 (GSE79899/GSM2108046; ref. 91), and HEL (GSE109492/GSM2944364; ref. 42), and mapped to the human genome (hg19) using Bowtie2 software with sensitive settings (92). Duplicate reads were removed prior to peak calling using MACS2 software using 5% FDR cutoff and broad peak option (93). Sequencing depth normalized ChIP-seq pileup tracks were visualized using the Integrative Genomics Viewer genome browser (94).

Statistical Analysis

Error bars represent the mean plus or minus SEM, and n refers to the number of biological repeats. Statistical significance was evaluated by P value using GraphPad Prism software or Scipy package from Python 3.8.5, as indicated in the figure legends. For Kaplan–Meier survival curves, the log-rank (Mantel–Cox) test was used to estimate median overall survival and statistical significance.

Authors' Disclosures

S.V. Iyer reports travel bursaries from Oxford Nanopore Technologies to cover expenses (travel, registration fees, food, etc.) incurred at conferences and presented talks/posters in the past. O. Klingbeil reports other support from Deutsche Forschungsgemeinschaft during the conduct of the study. W.R. McCombie reports grants from the NIH during the conduct of the study, as well as nonfinancial support from Pacific Bioscience, personal fees and other support from Orion

Genomics, and nonfinancial support and other support from Oxford Nanopore Technologies outside the submitted work. C.R. Vakoc reports grants from Boehringer Ingelheim during the conduct of the study; grants and personal fees from Syros Pharmaceuticals, grants from Treeline Biosciences, and personal fees from Flare Therapeutics, KSQ Therapeutics, Roivant Sciences, and C4 Therapeutics outside the submitted work; and owns a stock option in Treeline Biosciences. No disclosures were reported by the other authors.

Authors' Contributions

Y. Wei: Conceptualization, investigation, methodology, writing–original draft, writing–review and editing. **Y.-H. Huang:** Investigation. **D.S. Skopelitis:** Investigation. **S.V. Iyer:** Investigation, methodology. **A.S.H. Costa:** Investigation, methodology. **Z. Yang:** Investigation. **M. Kramer:** Investigation. **E.R. Adelman:** Investigation. **O. Klingbeil:** Investigation, methodology. **O.E. Demerdash:** Investigation. **S.A. Polyanskaya:** Investigation. **K. Chang:** Investigation. **S. Goodwin:** Investigation. **E. Hodges:** Supervision, investigation. **W.R. McCombie:** Supervision, investigation. **M.E. Figueroa:** Supervision, investigation. **C.R. Vakoc:** Conceptualization, supervision, writing–review and editing.

Acknowledgments

We thank James C. Mulloy for sharing genetically engineered human AML cell lines. The results analyzing patient data published here are in part based upon data generated by the TCGA Research Network: https://www.cancer.gov/tcga. This work was supported by Cold Spring Harbor Laboratory NCI Cancer Center Support grant 5P30CA045508. Additional funding was provided to C.R. Vakoc by the Pershing Square Sohn Cancer Research Alliance, NIH grants R01 CA174793 and P01 CA013106, and a Leukemia & Lymphoma Society Scholar Award. M.E. Figueroa is partially supported by a Scholar Award from the Leukemia & Lymphoma Society and by a Leukemia & Lymphoma Society SCOR award (7071-18). E.R. Adelman was supported by the T32-CA217835 Cancer Epigenetics Training grant to the University of Miami (Miami, FL).

The costs of publication of this article were defrayed in part by the payment of page charges. This article must therefore be hereby marked *advertisement* in accordance with 18 U.S.C. Section 1734 solely to indicate this fact.

Received December 24, 2020; revised June 25, 2021; accepted September 13, 2021; published first September 16, 2021.

REFERENCES

1. DeBerardinis RJ, Chandel NS. Fundamentals of cancer metabolism. Sci Adv 2016;2:e1600200.
2. Garcia-Bermudez J, Williams RT, Guarecuco R, Birsoy K. Targeting extracellular nutrient dependencies of cancer cells. Mol Metab 2020; 33:67–82.
3. Possemato R, Marks KM, Shaul YD, Pacold ME, Kim D, Birsoy K, et al. Functional genomics reveal that the serine synthesis pathway is essential in breast cancer. Nature 2011;476:346–50.
4. Wise DR, DeBerardinis RJ, Mancuso A, Sayed N, Zhang XY, Pfeiffer HK, et al. Myc regulates a transcriptional program that stimulates mitochondrial glutaminolysis and leads to glutamine addiction. Proc Natl Acad Sci U S A 2008;105:18782–7.
5. Cramer SL, Saha A, Liu J, Tadi S, Tiziani S, Yan W, et al. Systemic depletion of L-cyst(e)ine with cyst(e)inase increases reactive oxygen species and suppresses tumor growth. Nat Med 2017;23:120–7.
6. Peng H, Shen N, Qian L, Sun XL, Koduru P, Goodwin LO, et al. Hypermethylation of CpG islands in the mouse asparagine synthetase gene: relationship to asparaginase sensitivity in lymphoma cells. Partial methylation in normal cells. Br J Cancer 2001;85:930–5.
7. Jaffe N, Traggis D, Das L, Moloney WC, Hann HW, Kim BS, et al. L-asparaginase in the treatment of neoplastic diseases in children. Cancer Res 1971;31:942–9.
8. Nicholson LJ, Smith PR, Hiller L, Szlosarek PW, Kimberley C, Sehouli J, et al. Epigenetic silencing of argininosuccinate synthetase confers resistance to platinum-induced cell death but collateral sensitivity to arginine auxotrophy in ovarian cancer. Int J Cancer 2009;125: 1454–63.
9. Garcia-Bermudez J, Baudrier L, Bayraktar EC, Shen Y, La K, Guarecuco R, et al. Squalene accumulation in cholesterol auxotrophic lymphomas prevents oxidative cell death. Nature 2019;567:118–22.
10. Nakanishi T, Tamai I. Solute carrier transporters as targets for drug delivery and pharmacological intervention for chemotherapy. J Pharm Sci 2011;100:3731–50.
11. Bai X, Moraes TF, Reithmeier RAF. Structural biology of solute carrier (SLC) membrane transport proteins. Mol Membr Biol 2017;34:1–32.
12. Ganapathy V, Thangaraju M, Prasad PD. Nutrient transporters in cancer: relevance to Warburg hypothesis and beyond. Pharmacol Ther 2009;121:29–40.
13. Bacci M, Lorito N, Ippolito L, Ramazzotti M, Luti S, Romagnoli S, et al. Reprogramming of amino acid transporters to support aspartate and glutamate dependency sustains endocrine resistance in breast cancer. Cell Rep 2019;28:104–18.
14. El-Gebali S, Bentz S, Hediger MA, Anderle P. Solute carriers (SLCs) in cancer. Mol Aspects Med 2013;34:719–34.
15. Lin L, Yee SW, Kim RB, Giacomini KM. SLC transporters as therapeutic targets: emerging opportunities. Nat Rev Drug Discov 2015;14:543–60.
16. Zhang Y, Zhang Y, Sun K, Meng Z, Chen L. The SLC transporter in nutrient and metabolic sensing, regulation, and drug development. J Mol Cell Biol 2019;11:1–13.
17. Nyquist MD, Prasad B, Mostaghel EA. Harnessing solute carrier transporters for precision oncology. Molecules 2017;22:539.
18. Hu K, Li K, Lv J, Feng J, Chen J, Wu H, et al. Suppression of the SLC7A11/glutathione axis causes synthetic lethality in KRAS-mutant lung adenocarcinoma. J Clin Invest 2020;130:1752–66.
19. Holub BJ. Metabolism and function of myo-inositol and inositol phospholipids. Annu Rev Nutr 1986;6:563–97.
20. Croze ML, Soulage CO. Potential role and therapeutic interests of myo-inositol in metabolic diseases. Biochimie 2013;95:1811–27.
21. Martelli AM, Evangelisti C, Chiarini F, McCubrey JA. The phosphatidylinositol 3-kinase/Akt/mTOR signaling network as a therapeutic target in acute myelogenous leukemia patients. Oncotarget 2010;1:89–103.
22. Berridge MJ, Irvine RF. Inositol phosphates and cell signalling. Nature 1989;341:197–205.
23. Bansal VS, Majerus PW. Phosphatidylinositol-derived precursors and signals. Annu Rev Cell Biol 1990;6:41–67.
24. Nakanishi T, Balaban RS, Burg MB. Survey of osmolytes in renal cell lines. Am J Physiol 1988;255:C181–91.
25. Kitamura H, Yamauchi A, Nakanishi T, Takamitsu Y, Sugiura T, Akagi A, et al. Effects of inhibition of myo-inositol transport on MDCK cells under hypertonic environment. Am J Physiol 1997;272: F267–72.
26. Eisenberg F, Bolden AH. Biosynthesis of inositol in rat testis homogenate. Biochem Biophys Res Commun 1963;12:72–7.
27. Hauser G, Finelli VN. The biosynthesis of free and phosphatide myo-inositol from glucose by mammalian tissue slices. J Biol Chem 1963;238:3224–8.
28. Irvine RF, Schell MJ. Back in the water: the return of the inositol phosphates. Nat Rev Mol Cell Biol 2001;2:327–38.
29. Schneider S. Inositol transport proteins. FEBS Lett 2015;589:1049–58.
30. Stein AJ, Geiger JH. The crystal structure and mechanism of 1-L-myo-inositol-1-phosphate synthase. J Biol Chem 2002;277:9484–91.
31. Kwon HM, Yamauchi A, Uchida S, Preston AS, Garcia-Perez A, Burg MB, et al. Cloning of the cDNa for a Na+/myo-inositol cotransporter, a hypertonicity stress protein. J Biol Chem 1992;267:6297–301.
32. Hitomi K, Tsukagoshi N. cDNA sequence for rkST1, a novel member of the sodium ion-dependent glucose cotransporter family. Biochim Biophys Acta 1994;1190:469–72.

33. Uldry M, Ibberson M, Horisberger JD, Chatton JY, Riederer BM, Thorens B. Identification of a mammalian H(+)-myo-inositol symporter expressed predominantly in the brain. EMBO J 2001;20:4467–77.
34. Berry GT, Mallee JJ, Kwon HM, Rim JS, Mulla WR, Muenke M, et al. The human osmoregulatory Na+/myo-inositol cotransporter gene (SLC5A3): molecular cloning and localization to chromosome 21. Genomics 1995;25:507–13.
35. Hager K, Hazama A, Kwon HM, Loo DD, Handler JS, Wright EM. Kinetics and specificity of the renal Na+/myo-inositol cotransporter expressed in Xenopus oocytes. J Membr Biol 1995;143:103–13.
36. Roll P, Massacrier A, Pereira S, Robaglia-Schlupp A, Cau P, Szepetowski P. New human sodium/glucose cotransporter gene (KST1): identification, characterization, and mutation analysis in ICCA (infantile convulsions and choreoathetosis) and BFIC (benign familial infantile convulsions) families. Gene 2002;285:141–8.
37. Coady MJ, Wallendorff B, Gagnon DG, Lapointe JY. Identification of a novel Na+/myo-inositol cotransporter. J Biol Chem 2002;277:35219–24.
38. Rossiter NJ, Huggler KS, Adelmann CH, Keys HR, Soens RW, Sabatini DM, et al. CRISPR screens in physiologic medium reveal conditionally essential genes in human cells. Cell Metab 2021;33:1248–63.
39. Lu B, Klingbeil O, Tarumoto Y, Somerville TDD, Huang Y-H, Wei Y, et al. A transcription factor addiction in leukemia imposed by the MLL promoter sequence. Cancer Cell 2018;34:970–81.
40. Brien GL, Remillard D, Shi J, Hemming ML, Chabon J, Wynne K, et al. Targeted degradation of BRD9 reverses oncogenic gene expression in synovial sarcoma. Elife 2018;7:e41305.
41. Lan X, Khandros E, Huang P, Peslak SA, Bhardwaj SK, Grevet JD, et al. The E3 ligase adaptor molecule SPOP regulates fetal hemoglobin levels in adult erythroid cells. Blood Adv 2019;3:1586–97.
42. Tarumoto Y, Lu B, Somerville TDD, Huang YH, Milazzo JP, Wu XS, et al. LKB1, salt-inducible kinases, and MEF2C are linked dependencies in acute myeloid leukemia. Mol Cell 2018;69:1017–27.
43. Grevet JD, Lan X, Hamagami N, Edwards CR, Sankaranarayanan L, Ji X, et al. Domain-focused CRISPR screen identifies HRI as a fetal hemoglobin regulator in human erythroid cells. Science 2018;361:285–90.
44. Oldenborg PA, Zheleznyak A, Fang YF, Lagenaur CF, Gresham HD, Lindberg FP. Role of CD47 as a marker of self on red blood cells. Science 2000;288:2051–4.
45. Blazar BR, Lindberg FP, Ingulli E, Panoskaltsis-Mortari A, Oldenborg PA, Iizuka K, et al. CD47 (integrin-associated protein) engagement of dendritic cell and macrophage counterreceptors is required to prevent the clearance of donor lymphohematopoietic cells. J Exp Med 2001;194:541–9.
46. Sick E, Jeanne A, Schneider C, Dedieu S, Takeda K, Martiny L. CD47 update: a multifaceted actor in the tumour microenvironment of potential therapeutic interest. Br J Pharmacol 2012;167:1415–30.
47. Burger JA, Kipps TJ. CXCR4: a key receptor in the crosstalk between tumor cells and their microenvironment. Blood 2006;107:1761–7.
48. Meacham CE, Lawton LN, Soto-Feliciano YM, Pritchard JR, Joughin BA, Ehrenberger T, et al. A genome-scale in vivo loss-of-function screen identifies Phf6 as a lineage-specific regulator of leukemia cell growth. Genes Dev 2015;29:483–8.
49. Meyers RM, Bryan JG, McFarland JM, Weir BA, Sizemore AE, Xu H, et al. Computational correction of copy number effect improves specificity of CRISPR-Cas9 essentiality screens in cancer cells. Nat Genet 2017;49:1779–84.
50. Dempster JM, Rossen J, Kazachkova M, Pan J, Kugener G, Root DE, et al. Extracting biological insights from the Project Achilles Genome-Scale CRISPR screens in cancer cell lines. bioRxiv 720243 [Preprint]. 2019. Available from: https://doi.org/10.1101/720243.
51. Berry GT, Wu S, Buccafusca R, Ren J, Gonzales LW, Ballard PL, et al. Loss of murine Na+/myo-inositol cotransporter leads to brain myo-inositol depletion and central apnea. J Biol Chem 2003;278:18297–302.
52. Chau JFL, Lee MK, Law JWS, Chung SK, Chung SSM. Sodium/myo-inositol cotransporter-1 is essential for the development and function of the peripheral nerves. FASEB J 2005;19:1887–9.
53. Moyer JD, Malinowski N, Napier EA, Strong J. Uptake and metabolism of myo-inositol by L1210 leukaemia cells. Biochem J 1988;254:95–100.
54. Hodges E, Molaro A, Dos Santos CO, Thekkat P, Song Q, Uren PJ, et al. Directional DNA methylation changes and complex intermediate states accompany lineage specificity in the adult hematopoietic compartment. Mol Cell 2011;44:17–28.
55. Cancer Genome Atlas Research Network, Ley TJ, Miller C, Ding L, Raphael BJ, Mungall AJ, et al. Genomic and epigenomic landscapes of adult de novo acute myeloid leukemia. N Engl J Med 2013;368:2059–74.
56. Glass JL, Hassane D, Wouters BJ, Kunimoto H, Avellino R, Garrett-Bakelman FE, et al. Epigenetic identity in AML depends on disruption of nonpromoter regulatory elements and is affected by antagonistic effects of mutations in epigenetic modifiers. Cancer Discov 2017;7:868–83.
57. Livermore TM, Azevedo C, Kolozsvari B, Wilson MSC, Saiardi A. Phosphate, inositol and polyphosphates. Biochem Soc Trans 2016;44:253–9.
58. Steger DJ, Haswell ES, Miller AL, Wente SR, O'Shea EK. Regulation of chromatin remodeling by inositol polyphosphates. Science 2003;299:114–6.
59. Szlosarek PW, Klabatsa A, Pallaska A, Sheaff M, Smith P, Crook T, et al. In vivo loss of expression of argininosuccinate synthetase in malignant pleural mesothelioma is a biomarker for susceptibility to arginine depletion. Clin Cancer Res 2006;12:7126–31.
60. Delage B, Luong P, Maharaj L, O'Riain C, Syed N, Crook T, et al. Promoter methylation of argininosuccinate synthetase-1 sensitises lymphomas to arginine deiminase treatment, autophagy and caspase-dependent apoptosis. Cell Death Dis 2012;3:e342.
61. Ren Y, Roy S, Ding Y, Iqbal J, Broome JD. Methylation of the asparagine synthetase promoter in human leukemic cell lines is associated with a specific methyl binding protein. Oncogene 2004;23:3953–61.
62. Touzart A, Lengliné E, Latiri M, Belhocine M, Smith C, Thomas X, et al. Epigenetic silencing affects l-asparaginase sensitivity and predicts outcome in T-ALL. Clin Cancer Res 2019;25:2483–93.
63. Ward PS, Patel J, Wise DR, Abdel-Wahab O, Bennett BD, Coller HA, et al. The common feature of leukemia-associated IDH1 and IDH2 mutations is a neomorphic enzyme activity converting alpha-ketoglutarate to 2-hydroxyglutarate. Cancer Cell 2010;17:225–34.
64. Figueroa ME, Abdel-Wahab O, Lu C, Ward PS, Patel J, Shih A, et al. Leukemic IDH1 and IDH2 mutations result in a hypermethylation phenotype, disrupt TET2 function, and impair hematopoietic differentiation. Cancer Cell 2010;18:553–67.
65. Yu W, Ye C, Greenberg ML. Inositol hexakisphosphate kinase 1 (IP6K1) regulates inositol synthesis in mammalian cells. J Biol Chem 2016;291:10437–44.
66. Zhou L, Sheng W, Jia C, Shi X, Cao R, Wang G, et al. Musashi2 promotes the progression of pancreatic cancer through a novel ISYNA1-p21/ZEB-1 pathway. J Cell Mol Med 2020;24:10560–72.
67. Koguchi T, Tanikawa C, Mori J, Kojima Y, Matsuda K. Regulation of myo-inositol biosynthesis by p53-ISYNA1 pathway. Int J Oncol 2016;48:2415–24.
68. Egler RA, Ahuja SP, Matloub Y. L-asparaginase in the treatment of patients with acute lymphoblastic leukemia. J Pharmacol Pharmacother 2016;7:62–71.
69. Shiue E, Prather KLJ. Improving D-glucaric acid production from myo-inositol in E. coli by increasing MIOX stability and myo-inositol transport. Metab Eng 2014;22:22–31.
70. Zheng S, Hou J, Zhou Y, Fang H, Wang TT, Liu F, et al. One-pot two-strain system based on glucaric acid biosensor for rapid screening of myo-inositol oxygenase mutations and glucaric acid production in recombinant cells. Metab Eng 2018;49:212–9.
71. Ramaley R, Fujita Y, Freese E. Purification and properties of Bacillus subtilis inositol dehydrogenase. J Biol Chem 1979;254:7684–90.
72. Kouzuma T, Takahashi M, Endoh T, Kaneko R, Ura N, Shimamoto K, et al. An enzymatic cycling method for the measurement of myo-inositol in biological samples. Clin Chim Acta 2001;312:143–51.
73. Mulloy JC, Wunderlich M, Zheng Y, Wei J. Transforming human blood stem and progenitor cells: a new way forward in leukemia modeling. Cell Cycle 2008;7:3314–9.
74. Wunderlich M, Mizukawa B, Chou FS, Sexton C, Shrestha M, Saunthararajah Y, et al. AML cells are differentially sensitive to

chemotherapy treatment in a human xenograft model. Blood 2013; 121:e90–7.
75. Tarumoto Y, Lin S, Wang J, Milazzo JP, Xu Y, Lu B, et al. Salt-inducible kinase inhibition suppresses acute myeloid leukemia progression in vivo. Blood 2020;135:56–70.
76. Shi J, Wang E, Milazzo JP, Wang Z, Kinney JB, Vakoc CR. Discovery of cancer drug targets by CRISPR-Cas9 screening of protein domains. Nat Biotechnol 2015;33:661–7.
77. Adamson B, Norman TM, Jost M, Cho MY, Nuñez JK, Chen Y, et al. A multiplexed single-cell CRISPR screening platform enables systematic dissection of the unfolded protein response. Cell 2016;167:1867–82.
78. Li W, Xu H, Xiao T, Cong L, Love MI, Zhang F, et al. MAGeCK enables robust identification of essential genes from genome-scale CRISPR/Cas9 knockout screens. Genome Biol 2014;15:554.
79. Li W, Köster J, Xu H, Chen C-H, Xiao T, Liu JS, et al. Quality control, modeling, and visualization of CRISPR screens with MAGeCK-VISPR. Genome Biol 2015;16:281.
80. Mackay GM, Zheng L, van den Broek NJF, Gottlieb E. Analysis of cell metabolism using LC-MS and isotope tracers. Meth Enzymol 2015;561:171–96.
81. Su X, Lu W, Rabinowitz JD. Metabolite spectral accuracy on orbitraps. Anal Chem 2017;89:5940–8.
82. Gilpatrick T, Lee I, Graham JE, Raimondeau E, Bowen R, Heron A, et al. Targeted nanopore sequencing with Cas9-guided adapter ligation. Nat Biotechnol 2020;38:433–8.
83. Iyer SV, Goodwin S, Kramer M, McCombie WR. Understanding genetic variation in cancer using targeted nanopore long read sequencing [abstract]. In: Proceedings of the Annual Meeting of the American Association for Cancer Research 2020; 2020 Apr 27–28 and Jun 22–24; Philadelphia (PA): AACR; 2020. Abstract nr 1360.
84. Simpson JT, Workman RE, Zuzarte PC, David M, Dursi LJ, Timp W. Detecting DNA cytosine methylation using nanopore sequencing. Nat Methods 2017;14:407–10.
85. Li H. Minimap2: pairwise alignment for nucleotide sequences. Bioinformatics 2018;34:3094–100.
86. Li H, Handsaker B, Wysoker A, Fennell T, Ruan J, Homer N, et al. The sequence alignment/Map format and SAMtools. Bioinformatics 2009;25:2078–9.
87. Cerami E, Gao J, Dogrusoz U, Gross BE, Sumer SO, Aksoy BA, et al. The cBio cancer genomics portal: an open platform for exploring multidimensional cancer genomics data. Cancer Discov 2012;2:401–4.
88. Gao J, Aksoy BA, Dogrusoz U, Dresdner G, Gross B, Sumer SO, et al. Integrative analysis of complex cancer genomics and clinical profiles using the cBioPortal. Sci Signal 2013;6:pl1.
89. Hoadley KA, Yau C, Hinoue T, Wolf DM, Lazar AJ, Drill E, et al. Cell-of-origin patterns dominate the molecular classification of 10,000 tumors from 33 types of cancer. Cell 2018;173:291–304.
90. Rathert P, Roth M, Neumann T, Muerdter F, Roe J-S, Muhar M, et al. Transcriptional plasticity promotes primary and acquired resistance to BET inhibition. Nature 2015;525:543–7.
91. Prange KHM, Mandoli A, Kuznetsova T, Wang SY, Sotoca AM, Marneth AE, et al. MLL-AF9 and MLL-AF4 oncofusion proteins bind a distinct enhancer repertoire and target the RUNX1 program in 11q23 acute myeloid leukemia. Oncogene 2017;36:3346–56.
92. Langmead B, Salzberg SL. Fast gapped-read alignment with Bowtie 2. Nat Methods 2012;9:357–9.
93. Feng J, Liu T, Qin B, Zhang Y, Liu XS. Identifying ChIP-seq enrichment using MACS. Nat Protoc 2012;7:1728–40.
94. Robinson JT, Thorvaldsdóttir H, Winckler W, Guttman M, Lander ES, Getz G, et al. Integrative genomics viewer. Nat Biotechnol 2011;29: 24–6.
95. Hart T, Chandrashekhar M, Aregger M, Steinhart Z, Brown KR, MacLeod G, et al. High-resolution CRISPR screens reveal fitness genes and genotype-specific cancer liabilities. Cell 2015;163:1515–26.
96. Ghandi M, Huang FW, Jané-Valbuena J, Kryukov GV, Lo CC, McDonald ER, et al. Next-generation characterization of the Cancer Cell Line Encyclopedia. Nature 2019;569:503–8.
97. Barretina J, Caponigro G, Stransky N, Venkatesan K, Margolin AA, Kim S, et al. The Cancer Cell Line Encyclopedia enables predictive modelling of anticancer drug sensitivity. Nature 2012;483:603–7.